Systemic HIV and SIV latency reversal via non-canonical NF-κB signalling in vivo

https://doi.org/10.1038/s41586-020-1951-3

Received: 12 April 2019

Accepted: 16 December 2019

Published online: 22 January 2020

Christopher C. Nixon[1,2,3,20], Maud Mavigner[4,20], Gavin C. Sampey[2,3,5,6], Alyssa D. Brooks[4], Rae Ann Spagnuolo[1,2,3], David M. Irlbeck[6,7], Cameron Mattingly[4], Phong T. Ho[1,2,3], Nils Schoof[4], Corinne G. Cammon[1,2,3], Greg K. Tharp[8], Matthew Kanke[9,10], Zhang Wang[11], Rachel A. Cleary[1,2,3], Amit A. Upadhyay[8], Chandrav De[1,2,3], Saintedym R. Wills[2,3,5,6], Shane D. Falcinelli[2,3,5,12], Cristin Galardi[6,7], Hasse Walum[8], Nathaniel J. Schramm[1,2,3], Jennifer Deutsch[11], Jeffrey D. Lifson[13], Christine M. Fennessey[13], Brandon F. Keele[13], Sherrie Jean[8], Sean Maguire[11], Baolin Liao[1,2,3,14], Edward P. Browne[2,3,5], Robert G. Ferris[6,7], Jessica H. Brehm[6,7], David Favre[6,11], Thomas H. Vanderford[8], Steven E. Bosinger[8,15], Corbin D. Jones[9,10], Jean-Pierre Routy[16,17], Nancie M. Archin[2,3,5], David M. Margolis[2,3,5,6,12,18], Angela Wahl[1,2,3], Richard M. Dunham[2,3,5,6,7,21]*, Guido Silvestri[8,15], Ann Chahroudi[4,8,19,21]* & J. Victor Garcia[1,2,3,21]*

Long-lasting, latently infected resting CD4$^+$ T cells are the greatest obstacle to obtaining a cure for HIV infection, as these cells can persist despite decades of treatment with antiretroviral therapy (ART). Estimates indicate that more than 70 years of continuous, fully suppressive ART are needed to eliminate the HIV reservoir[1]. Alternatively, induction of HIV from its latent state could accelerate the decrease in the reservoir, thus reducing the time to eradication. Previous attempts to reactivate latent HIV in preclinical animal models and in clinical trials have measured HIV induction in the peripheral blood with minimal focus on tissue reservoirs and have had limited effect[2–9]. Here we show that activation of the non-canonical NF-κB signalling pathway by AZD5582 results in the induction of HIV and SIV RNA expression in the blood and tissues of ART-suppressed bone-marrow–liver–thymus (BLT) humanized mice and rhesus macaques infected with HIV and SIV, respectively. Analysis of resting CD4$^+$ T cells from tissues after AZD5582 treatment revealed increased SIV RNA expression in the lymph nodes of macaques and robust induction of HIV in almost all tissues analysed in humanized mice, including the lymph nodes, thymus, bone marrow, liver and lung. This promising approach to latency reversal—in combination with appropriate tools for systemic clearance of persistent HIV infection—greatly increases opportunities for HIV eradication.

Latently infected cells carrying an integrated replication-competent provirus that contribute to viral rebound after the interruption of ART (termed the HIV reservoir) are not detected and eliminated by the immune system or current therapeutics. Therefore, the HIV reservoir has been targeted by approaches to reverse latency and induce viral antigen production (that is, 'HIV reactivation')[2–9], which renders infected cells susceptible to virus-induced cell death or clearance by the immune system. Previous approaches to HIV reactivation have been modestly effective and have not demonstrated reactivation of HIV in resting CD4$^+$ T cells in tissues[2–9].

HIV induction in vitro by SMAC mimetics

The lack of specificity of molecules that activate the NF-κB pathway as latency-reversal agents (LRAs) often leads to toxicities that prevent clinical implementation[10]. We tested the induction of HIV and

[1]International Center for the Advancement of Translational Science, University of North Carolina at Chapel Hill, Chapel Hill, NC, USA. [2]Division of Infectious Diseases, Department of Medicine, University of North Carolina at Chapel Hill, Chapel Hill, NC, USA. [3]Center for AIDS Research, University of North Carolina at Chapel Hill, Chapel Hill, NC, USA. [4]Department of Pediatrics, Emory University School of Medicine, Atlanta, GA, USA. [5]UNC HIV Cure Center, University of North Carolina at Chapel Hill, Chapel Hill, NC, USA. [6]Qura Therapeutics, Chapel Hill, NC, USA. [7]HIV Drug Discovery, ViiV Healthcare, Research Triangle Park, NC, USA. [8]Yerkes National Primate Research Center, Emory University, Atlanta, GA, USA. [9]Department of Biology, University of North Carolina at Chapel Hill, Chapel Hill, NC, USA. [10]Department of Genetics, University of North Carolina at Chapel Hill, Chapel Hill, NC, USA. [11]GlaxoSmithKline Research and Development, Collegeville, PA, USA. [12]Department of Microbiology and Immunology, School of Medicine, University of North Carolina at Chapel Hill, Chapel Hill, NC, USA. [13]AIDS and Cancer Virus Program, Frederick National Laboratory for Cancer Research, Frederick, MD, USA. [14]Department of Infectious Diseases, Guangzhou Eighth People's Hospital, Guangzhou Medical University, Guangzhou, China. [15]Department of Pathology and Laboratory Medicine, Emory University School of Medicine, Atlanta, GA, USA. [16]Chronic Viral Infection Service, McGill University Health Centre, Montreal, Quebec, Canada. [17]Division of Hematology, McGill University Health Centre, Montreal, Quebec, Canada. [18]Department of Epidemiology, Gillings School of Public Health, University of North Carolina at Chapel Hill, Chapel Hill, NC, USA. [19]Emory + Children's Center for Childhood Infections and Vaccines, Atlanta, GA, USA. [20]These authors contributed equally: Christopher C. Nixon, Maud Mavigner. [21]These authors jointly supervised this work: Richard M. Dunham, Ann Chahroudi, J. Victor Garcia. *e-mail: richard.m.dunham@viivhealthcare.com; ann.m.chahroudi@emory.edu; victor_garcia@med.unc.edu

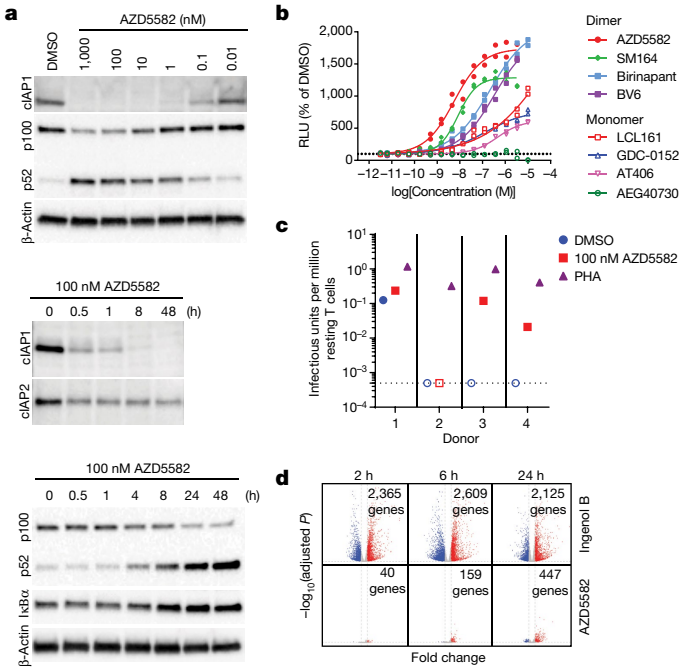

Fig. 1 | Efficient in vitro AZD5582 target engagement and induction of HIV transcription. a, Total CD4$^+$ T cells were treated with a broad range of concentrations (10 pM–1 μM) of AZD5582 overnight, and cell lysates were analysed by immunoblot, probing for cIAP1 and p100/p52 as indicated (top; representative of 10 experiments). Immunoblot analysis of isolated total CD4$^+$ T cell lysates after treatment with 100 nM AZD5582, examining components of the cNF-κB and ncNF-κB pathways over a 48-h time course after treatment (middle and bottom; representative of three and four experiments, respectively). **b**, DMSO-normalized reporter signal induced by a dose titration of a panel of mono- and bivalent SMAC mimetics in a Jurkat luciferase reporter model of HIV-1 latency with 48 h exposure. Symbols represent technical replicates from a single run and are representative of three independent experiments. Lines represent a four-parameter logistic-regression model fit. **c**, Infectious units per million resting CD4$^+$ T cells induced by DMSO or 100 nM AZD5582 were determined in a limiting dilution quantitative viral outgrowth assay. PHA, phytohaemagglutinin. **d**, Volcano plots summarizing mean up- and downregulated genes at 2, 6 and 24 h after treatment with ingenol B or AZD5582 compared with treatment with DMSO alone. The mean $\log_2$-transformed fold change is shown on the *x* axis and $\log_{10}$-adjusted *P* values (two-sided Wald test) are shown on the *y* axis. Dashed lines represent thresholds of $\log_2$-transformed fold change of 1 and adjusted $P < 0.05$. The data shown represent the mean fold change across four donors and one experiment. For gel source data, see Supplementary Fig. 1.

SIV transcription in latently infected cells by the non-canonical (nc) NF-κB pathway. This pathway activates a limited number of cellular genes and a more-gradual but persistent activation of NF-κB-driven transcription than the canonical (c)NF-κB pathway[11]. Mimetics of the second mitochondrial-derived activator of caspases (SMAC) activate the ncNF-κB pathway by inhibiting the cellular inhibitor of apoptosis protein 1 (cIAP1) and cIAP2. cIAP1 continually represses the ncNF-κB pathway by constitutively degrading the NF-κB-inducing kinase, thus preventing processing of p100 into p52[12]; this repression can be relieved in CD4$^+$ T cells by in vitro treatment with the SMAC mimetic AZD5582 (Fig. 1a and Extended Data Fig. 1). Compared with other SMAC mimetics, AZD5582 had a superior capacity to reverse HIV latency in vitro[13] (Fig. 1b). AZD5582 also induced replication-competent HIV expression in resting CD4$^+$ T cells from ART-suppressed HIV-infected donors (Fig. 1c). AZD5582 induced five- to tenfold fewer genes than the protein kinase C agonist ingenol B (Fig. 1d), a cNF-κB pathway inducer and activator of several transcription factors. By specifically targeting the ncNF-κB signalling pathway, AZD5582 has limited pleotropic effects, which may translate to fewer off-target effects[14].

Latency reversal in BLT humanized mice

BLT mice were infected with HIV-$1_{JR\text{-}CSF}$ (Supplementary Table 1) and suppressed with ART[15–18] (Fig. 2a, b). Mice then received a single intraperitoneal injection of 3 mg kg^{-1} AZD5582 or vehicle. No changes in plasma HIV RNA levels were detected in vehicle-control-treated mice at 24 or 48 h nor in AZD5582-treated mice 24 h after AZD5582 administration (Fig. 2c). However, 48 h after AZD5582 treatment increased HIV RNA expression was detected in the plasma of 3 out of 6 (50%) and 3 out of 4 (75%) mice in two independent experiments (Fig. 2c). These data demonstrate that a single dose of AZD5582 can induce HIV production, resulting in significant viraemia (up to 1,574 HIV RNA copies per ml plasma) in ART-treated BLT mice (Supplementary Table 2).

The hallmark of HIV persistence in humans is the presence of inducible HIV in resting CD4$^+$ T cells. Therefore, resting cells from primary (bone marrow and thymic organoid), secondary (lymph node and spleen) and effector (liver and lung) immune tissues were isolated from HIV-infected ART-suppressed BLT mice 48 h after treatment with vehicle control or AZD5582[17,19,20]. The levels of HIV RNA in resting CD4$^+$ T cells from AZD5582-treated mice were 11-fold (bone marrow, $P = 0.0201$), 21-fold (thymic organoid, $P = 0.0038$), 12-fold (lymph node, $P = 0.0004$), 1.4-fold (spleen, $P = 0.0426$), 24-fold (liver, $P = 0.0145$) and 3.2-fold (lung, $P = 0.0029$) higher than controls (Fig. 2d). These results were confirmed in a second independent experiment (Extended Data Fig. 2). No notable differences in cell-associated HIV DNA were noted between mice treated with vehicle control or AZD5582 (Supplementary Table 3). These results demonstrate that AZD5582 induces systemic HIV RNA production in resting CD4$^+$ T cells, indicative of latency reversal in this important cellular source of persistent HIV infection. We also isolated cells from the peripheral blood, female reproductive tract and brain of HIV-infected ART-suppressed BLT mice 48 h after treatment with AZD5582 or vehicle control. As too few CD4$^+$ T cells were available for cell sorting from these compartments, RNA was extracted from total cells and analysed for the presence of HIV RNA in each tissue. The levels of HIV RNA were significantly higher in the female reproductive tract (3.4-fold, $P = 0.0152$) and brain (8.7-fold, $P = 0.0147$) of AZD5582-treated mice compared with vehicle controls, but not in the blood ($P = 0.3095$) (Fig. 2e). Together, these results show that AZD5582 treatment induces systemic HIV RNA production in BLT mice.

Pharmacodynamics and safety in BLT mice

Target engagement after treatment with AZD5582 was confirmed ex vivo by the degradation of cIAP1 (proximal) and p100 (distal), targets of SMAC in the ncNF-κB pathway (Extended Data Fig. 3a). In vivo target engagement was demonstrated in resting CD4$^+$ T cells isolated from thymus, spleen, lymph nodes, liver, lung and bone marrow of BLT mice treated with a single dose of 3 mg kg^{-1} AZD5582 or vehicle control (Extended Data Fig. 3b). These results were confirmed by immunohistochemical analysis of the thymic organoid of HIV-infected ART-suppressed BLT mice. This analysis showed a marked reduction in cIAP1 expression in the thymic organoid of AZD5582-treated mice (Extended Data Fig. 3c).

To study off-target or immune-mediated toxicities of AZD5582, we measured serum chemistry, T cell activation and a panel of plasma cytokines after in vivo treatment of immunocompetent BALB/c mice. AZD5582 administration resulted in mild and transient increases in alanine aminotransferase and aspartate aminotransferase that resolved a few days after treatment. No other changes in serum chemistries were noted (Supplementary Table 4). In addition, no differences were noted in the levels of activated (CD38$^+$HLA-DR$^+$) CD4$^+$ or CD8$^+$ T cells in BLT mice treated with AZD5582 or vehicle control (Supplementary Table 5) or in plasma levels of 41 human cytokines and chemokines that serve as indicators of systemic

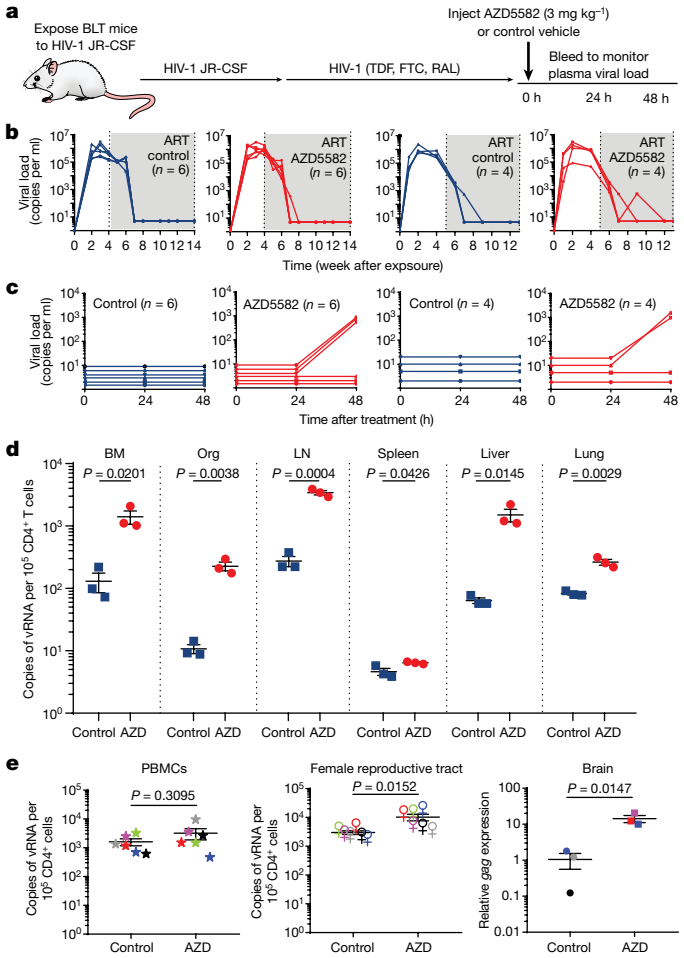

Fig. 2 | AZD5582 induces HIV RNA expression in resting CD4$^+$ T cells from tissues of HIV-infected ART-suppressed BLT mice. a, BLT mice were infected with HIV-$1_{JR\text{-}CSF}$. After 10 weeks of ART treatment, mice received vehicle control or AZD5582. FTC, emtricitabine; RAL, raltegravir; TDF, tenofovir disoproxil fumarate. **b**, HIV RNA copies per ml^{-1} of plasma of HIV-infected ART-treated BLT mice before treatment with vehicle control (left; blue lines) or AZD5582 (right; red lines). Two independent experiments were performed (left, $n = 6$ mice per group; right, $n = 4$ mice per group). Grey shading, period of ART administration. **c**, Plasma HIV RNA levels in HIV-infected ART-suppressed mice from **b** treated with vehicle control or AZD5582. **d**, HIV viral RNA (vRNA) levels in resting CD4$^+$ T cells isolated from the bone marrow (BM), thymic organoid (Org), lymph nodes (LN), spleen, liver and lung of control or AZD5582-treated mice (cells pooled from $n = 6$ mice per group for each tissue) were analysed in triplicate. Data are mean ± s.e.m. Statistical significance was determined using a two-sided Student's *t*-test. **e**, Cell-associated HIV RNA copies in the blood ($n = 6$), female reproductive tract ($n = 6$) and brain ($n = 3$). PBMCs, peripheral-blood mononuclear cells. Statistical significance was determined using a two-sided Mann–Whitney test (peripheral-blood mononuclear cells and female reproductive tract) or Student's *t*-test (brain). Colours indicate samples from the same mice. Data are mean ± s.e.m.

activation and inflammation[21] (Supplementary Table 6). Together, these results demonstrate that AZD5582 does not cause generalized toxicity or activation of the immune system in the BLT model.

Latency reversal in rhesus macaques

We next evaluated the latency-reversal activity of AZD5582 in 21 MamuB*08$^-$ and MamuB*17$^-$ rhesus macaques infected with SIV_{mac239} and treated with a potent ART regimen comprising tenofovir diso-proxil fumarate, emtricitabine and dolutegravir initiated 8 weeks after infection (Fig. 3a and Supplementary Table 7)[22,23]. Suppression of SIV viraemia below 60 copies per ml (standard assay limit of detection) was achieved in all macaques in 2–20 weeks and ART was continued for 55–67 weeks before further treatment (Fig. 3b). On the basis of pharmacokinetic and pharmacodynamic data from uninfected macaques (Extended Data Fig. 4a) as well as protocols for SMAC mimetics used in oncology, intravenous infusions of 0.1 mg kg^{-1} AZD5582 were administered weekly to 12 SIV-infected ART-suppressed rhesus macaques for 3 or 10 weeks (Fig. 3a). Nine SIV-infected ART-suppressed rhesus macaques served as controls (Fig. 3a). Plasma concentrations of AZD5582 measured after the first, third, sixth and tenth dose showed that drug exposures in SIV-infected ART-suppressed macaques were consistent across the treatment period and comparable to those observed in uninfected rhesus macaques (Extended Data Fig. 4b).

Latency reversal, defined as on-ART viraemia increasing from less than 60 copies per ml of plasma to more than 60 copies per ml of plasma after AZD5582 treatment, was observed as early as 96 h after the first dose and reached levels as high as 1,390 copies per ml in SIV-infected rhesus macaques (Fig. 3c, d). On-ART viraemia >60 copies per ml of plasma was observed in 5 out of 12 rhesus macaques (42%), corresponding to 5 out of 9 rhesus macaques (55%) that received 10 doses of AZD5582 (Fig. 3c, d). Multiple instances of sustained viraemia >60 copies per ml between AZD5582 doses were observed. Out of 140 viral load measurements performed on the 5 macaques that exhibited on-ART viraemia during AZD5582 treatment, 64 were >60 copies per ml (46%); in the macaque with the greatest frequency of reactivation, this proportion was 15 out of 28 (53%). Longitudinal examination of plasma virus by single-genome sequencing analysis of the SIV_{mac239} *env* gene in all rhesus macaques that experienced AZD5582-induced on-ART viraemia was performed at four selected time points: 2 weeks after infection (near peak viraemia), 8 weeks after infection (immediately before ART initiation), and at 2 time points separated by 26–42 days during AZD5582 treatment. Phylogenetic analyses showed several patterns of virus reactivation (Extended Data Fig. 5). In two rhesus macaques (RDl16 and RKn16), most of the reactivated virus sequences were phylogenetically closer to sequences at eight weeks after infection rather than peak viraemia and were unique, indicating that the variants produced during AZD5582 treatment originated from multiple cells that were seeded at the time of ART initiation[24]. In two other rhesus macaques (RKl16 and RDm16), a large fraction of the viruses produced during AZD5582 treatment showed identical sequences, suggesting that latency reversal occurred from a single cell or a clonally expanded population of infected cells. These clones clustered with both peak and pre-ART time points and were accompanied by additional unique sequences. In one rhesus macaque (RLy15), a single virus sequence was amplified at each time point during AZD5582 treatment and these were both phylogenetically similar to sequences found before ART treatment. Taken together, these results indicate that AZD5582 induced virus reactivation from a diverse population of cells, some of which may be clonally expanded[25,26].

We quantified cell-associated SIV RNA and SIV DNA in resting CD4$^+$ T cells sorted from SIV-infected ART-suppressed rhesus macaques treated or not with AZD5582. Cell-associated SIV RNA levels in resting CD4$^+$ T cells isolated from lymph nodes were significantly higher in macaques who received ten doses of AZD5582 compared with controls ($P = 0.0148$) (Fig. 3e). A similar trend was observed in resting CD4$^+$ T cells isolated from the spleens of a subgroup of six macaques that were euthanized. Levels of cell-associated SIV DNA in resting CD4$^+$ T cells were similar in each compartment across groups (Fig. 3e). To further understand whether latency reversal induced by AZD5582 resulted in a perturbation of the overall level of infected CD4$^+$ T cells, we performed longitudinal measurements of cell-associated SIV DNA in total (rather than resting) CD4$^+$ T cells isolated from lymph nodes and blood as well as quantitative viral outgrowth assays using CD4$^+$ T cells from lymph nodes and spleen at the end of the treatment period (Extended

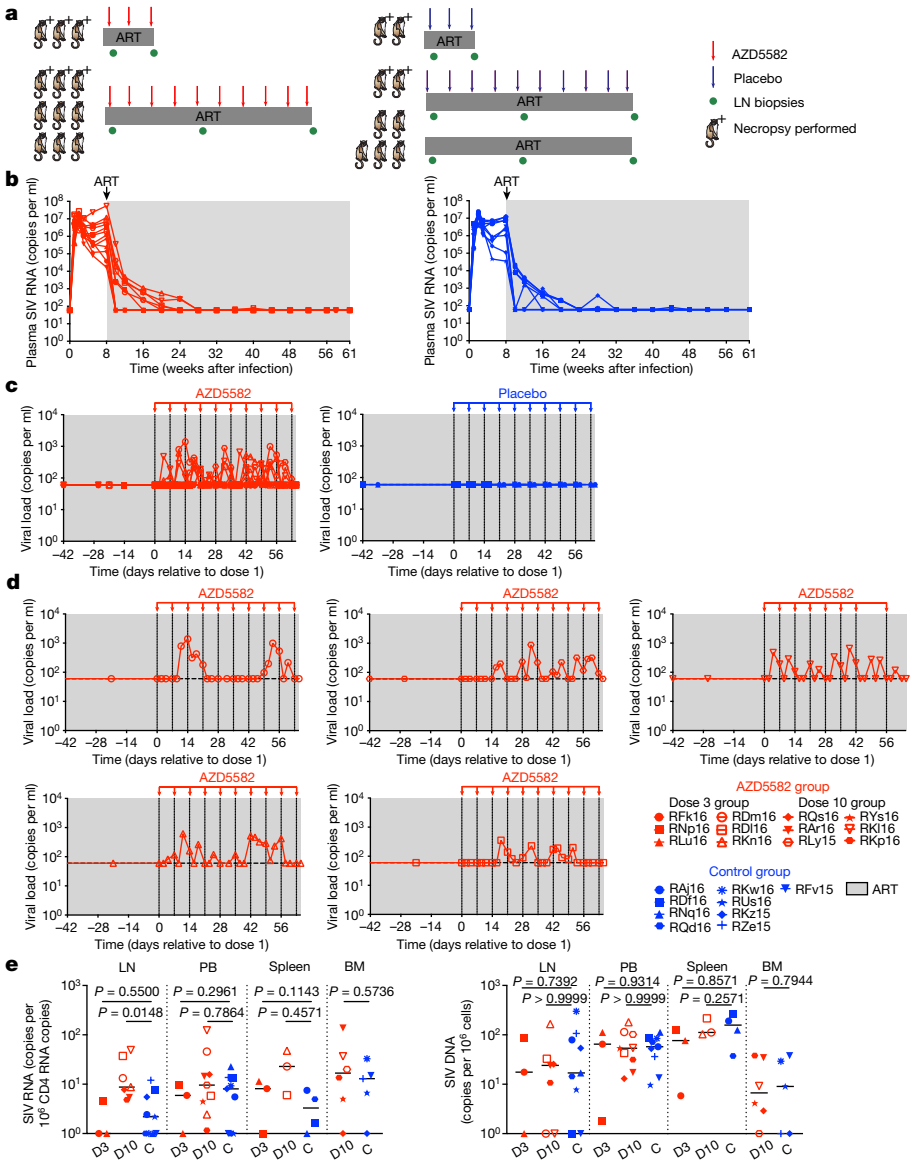

Fig. 3 | AZD5582 induces SIV RNA expression in the plasma and lymph nodes of ART-suppressed SIV-infected rhesus macaques. a, Experimental design during AZD5582 treatment phase. Three rhesus macaques received three doses of AZD5582 and were euthanized 48 h after the last dose. Nine rhesus macaques received 10 doses of AZD5582 and 3 were euthanized 48 h after the last dose. The first dose of AZD5582 was administered after 55–67 weeks of ART (3-dose group, 55 weeks; 10-dose group, 55–67 weeks). Four control rhesus macaques received a weekly placebo infusion; 2 were euthanized 48 h after 3 infusions and 2 were euthanized 48 h after 10 infusions. Five control macaques received ART only. **b**, Plasma SIV RNA levels in the 21 SIV-infected rhesus macaques before treatment with AZD5582 (left, $n = 12$) and equivalent time period for controls (right, $n = 9$). **b**–**d**, Grey shading represents the period of ART administration. **c**, Plasma SIV RNA levels in ART-suppressed SIV-infected rhesus macaques during AZD5582 treatment (left, $n = 12$) and the equivalent time period for controls (right, $n = 9$). **d**, Individual representation of plasma SIV RNA levels in the five rhesus macaques that experienced on-ART viraemia during AZD5582 treatment. **e**, Cell-associated SIV RNA (left) and SIV DNA (right) levels in resting $CD4^+$ T cells isolated from lymph nodes, peripheral blood (PB), spleen and bone marrow of AZD5582-treated (red) and control (blue) ART-suppressed SIV-infected rhesus macaques. Resting $CD4^+$ T cells were analysed from AZD5582-treated rhesus macaques 48 h after receiving 3 doses (D3; lymph nodes, peripheral blood and spleen, $n = 3$) or 10 doses (D10; lymph nodes, $n = 7$; peripheral blood, $n = 9$; spleen, $n = 3$; bone marrow, $n = 6$) of AZD5582. Resting $CD4^+$ T cells were analysed from control rhesus macaques (C; lymph nodes and peripheral blood, $n = 9$; spleen, $n = 4$; bone marrow, $n = 5$) at equivalent time points. Open symbols indicate AZD5582-treated rhesus macaques with on-ART viraemia. Statistical significance was determined with a two-sided Mann–Whitney *U*-test. Horizontal lines represent the median.

Data Fig. 6a–c). Despite the high level of virus reactivation induced by AZD5582, these experiments did not reveal a consistent reduction in the total or replication-competent SIV reservoir compared with controls.

Pharmacodynamics in rhesus macaques

Pharmacological target engagement of the ncNF-κB pathway was confirmed by western blot analysis of the degradation of p100 to p52 in lymph-node mononuclear cells after in vivo exposure to AZD5582 (Extended Data Fig. 4c) and in splenocytes treated ex vivo with AZD5582 (Extended Data Fig. 4d–g). Transcriptomic profiling of $CD4^+$ T cells from the peripheral blood and lymph nodes isolated from AZD5582-treated rhesus macaques showed a distinct effect of AZD5582 on gene expression based on principal component (Fig. 4a) and DAVID pathway (Extended Data Fig. 7a) analyses. Enrichment of NF-κB targets after AZD5582 treatment was demonstrated by gene-set enrichment analysis

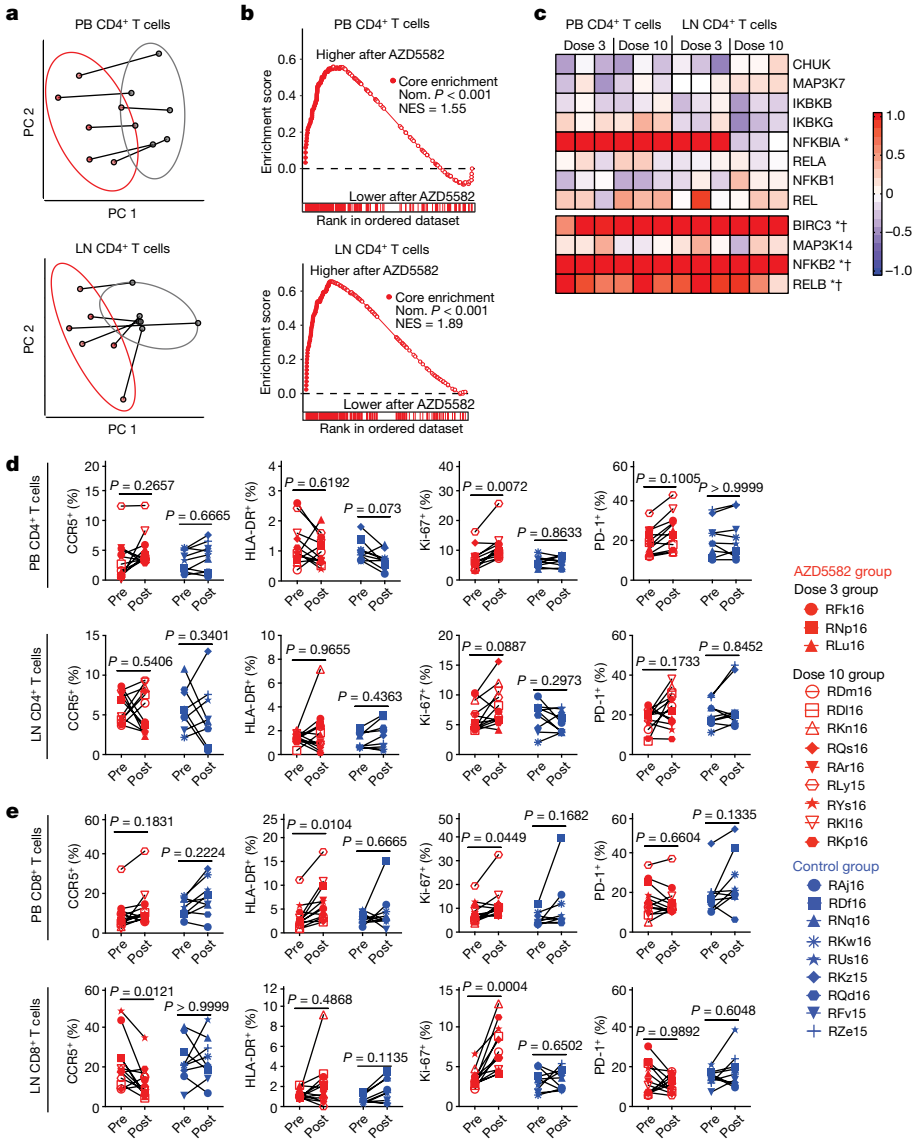

Fig. 4 | AZD5582 specifically activates the ncNF-κB pathway in SIV-infected ART-suppressed rhesus macaques without generalized T cell activation. **a**–**c**, Gene expression in CD4+ T cells from the peripheral blood and lymph nodes of SIV-infected ART-suppressed rhesus macaques before and after treatment with AZD5582 ($n = 6$ for both lymph nodes and peripheral blood; for each, $n = 3$ for 3 doses of AZD5582 and $n = 3$ for 10 doses of AZD5582). **a**, Principal component (PC) analyses of the transcriptomes of CD4+ T cells from the peripheral blood (top) and lymph nodes (bottom), before (grey) and after (red) treatment with AZD5582. Ellipses, two standard deviations. **b**, GSEA plots of NF-κB-induced genes in CD4+ T cells from the peripheral blood (top) and lymph nodes (bottom). Gene set: 'hallmark TNF signalling via NF-κB' (MSigDB). NES, normalized enrichment score. **c**, Heat map of cNF-κB (top) and ncNF-κB (bottom) pathway gene expression. Colour scale, $\log_2$-transformed fold changes after AZD5582 treatment compared with before treatment. Genes that are differentially expressed after treatment with AZD5582 in the peripheral blood (asterisks) or lymph nodes (daggers) CD4+ T cells are highlighted. **d**, **e**, Expression of activation markers in CD4+ (**d**) and CD8+ (**e**) T cells in the peripheral blood (top) and lymph nodes (bottom) of SIV-infected ART-suppressed rhesus macaques before treatment with AZD5582 and 48 h after the final dose ($n = 12$, red) and control rhesus macaques ($n = 9$, blue). Statistical significance was determined using a two-sided Mann–Whitney U-test.

(GSEA) (Fig. 4b; a heat map of differentially expressed gene targets of NF-κB is shown in Extended Data Fig. 7b). The hallmark ncNF-κB signalling genes *NFKB2* and *RELB* were significantly upregulated in CD4+ T cells from the peripheral blood and lymph nodes after AZD5582 treatment, whereas cNF-κB signalling molecules were mostly unaffected except for the inhibitor NFKBIA (Fig. 4c). The baculoviral IAP repeat-containing 3 (*BIRC3*) gene, which encodes cIAP2 and regulates both the cNF-κB and ncNF-κB pathways, was also significantly upregulated in CD4+ T cells from the peripheral blood and lymph nodes (Fig. 4c). Notably, activation of ncNF-κB signalling genes was evident in rhesus macaques with and without on-ART viraemia of more than 60 copies per ml (Fig. 4c and Extended Data Fig. 7c) and GSEA showed similar changes in overall gene expression when AZD5582-treated rhesus macaques were grouped according to the presence or absence of on-ART viraemia of more than 60 copies per ml (Supplementary Table 8), suggesting that the lack of a virological response measured by the standard viral load assay was not due to compromised target engagement.

We next used an ultrasensitive assay to measure SIV RNA in plasma, comparing 2–3 baseline time points during ART in the 4 weeks before AZD5582 treatment (when plasma SIV RNA was less than 60 copies per ml in all rhesus macaques using the standard viral load assay) and 3–4 time points during AZD5582 treatment (Extended Data Fig. 8a). We found significantly higher plasma SIV RNA values during the period of AZD5582 treatment compared with pre-treatment (Extended Data Fig. 8b, $P = 0.008$), with 8 out of 12 rhesus macaques demonstrating ≥2 SIV RNA measurements above the median of their baseline values. This group of eight rhesus macaques with evidence of latency reversal induced by AZD5582 could be segregated from the four rhesus macaques with unchanged viral loads based on two parameters: higher levels of plasma SIV RNA immediately before ART initiation and SIV DNA in peripheral CD4+ T cells before AZD5582 treatment ($P = 0.004$ for each) (Extended Data Fig. 8c).

Safety and immune effects in rhesus macaques

The potential for AZD5582 toxicity in SIV-infected ART-suppressed rhesus macaques was examined and transient increases in liver enzymes (aspartate aminotransferase and γ-glutamyltransferase) were observed (Extended Data Fig. 9a). Total white-blood cell counts were decreased in all rhesus macaques 48 h after the first dose of AZD5582 but returned to normal levels when measured before the second dose and over time (Extended Data Fig. 9b). After the seventh and eighth doses, one macaque experienced a reaction characterized by fever, emesis, fatigue and lack of appetite, and had elevated liver enzyme and creatinine levels and bandaemia as shown by laboratory examination. All abnormalities resolved within a two-week period; however, this rhesus macaque did

not receive further doses. Notably, weights did not significantly fluctuate over the course of the treatment period (Extended Data Fig. 9c). In summary, 97 doses of AZD5582 were administered to 12 SIV-infected ART-suppressed rhesus macaques, of which 95 were well-tolerated and 2 resulted in a mild adverse reaction.

Markers of T cell activation (both $CD4^+$ and $CD8^+$) were assessed in AZD5582-treated rhesus macaques and controls, and expression of CCR5, HLA-DR and PD-1 on $CD4^+$ T cells from the blood and lymph nodes was similar before and after treatment with AZD5582 (Fig. 4d, e). Levels of intracellular Ki-67 expression were increased in $CD4^+$ T cells in the blood and $CD8^+$ T cells in the blood and lymph nodes after AZD5582 treatment (Fig. 4d, e). $CD8^+$ T cell expression of HLA-DR was higher in the blood after exposure to AZD5582 (Fig. 4e). These results indicate that AZD5582 does not induce global $CD4^+$ T cell activation in rhesus macaques but the combined pharmacological and virological effects may have a stimulatory effect on $CD8^+$ T cells. Longitudinal analyses of $CD4^+$ T cell counts and frequencies, $CD4^+$ T cell viability, $CD4^+$ T cell subset frequencies and their Ki-67 expression are shown in Extended Data Fig. 10a–d. The increased Ki-67 observed within $CD4^+$ T cells after AZD5582 treatment may provide a note of caution as the proliferation of latently infected memory $CD4^+$ T cells is hypothesized to contribute to the maintenance of the viral reservoir over time[25,27]; however, we did not find an increase in infected cells after AZD5582 treatment (Fig. 3e and Extended Data Fig. 6).

We next determined whether AZD5582 would impair SIV-specific T cell responses in SIV-infected ART-suppressed rhesus macaques, a potential adverse outcome of treatment that has been suggested for other LRAs[28]. However, the frequency of SIV Gag- or Env-specific $CD8^+$ T cells measured by IFNγ ELISPOT did not decrease after AZD5582 treatment (Extended Data Fig. 10e), and $CD8^+$ T cell polyfunctionality and proliferative responses were largely unaffected by AZD5582 treatment ex vivo, with the exception of $IL\text{-}2^+IFN\gamma^+TNF^+$ triple-positive cells, which were slightly reduced ($P = 0.0476$) (Extended Data Fig. 10f, g). Furthermore, longitudinal assessment of plasma levels of inflammatory cytokines and chemokines did not reveal any marked changes induced by AZD5582 (Extended Data Fig. 10h). Overall, our work in the rhesus macaque model indicates that AZD5582 treatment is safe in most macaques and can induce appreciable increases in plasma SIV RNA as well as SIV RNA expression in resting $CD4^+$ T cells from the lymph nodes during ART.

Discussion

Eradication of HIV infection after prolonged viral suppression is the focus of intense research and latency reversal has been a cornerstone of this effort. LRAs have been widely recognized as important (but previously mostly theoretical) tools to induce HIV expression in resting $CD4^+$ T cells in humans. Future clinical applications of HIV cure strategies must be relevant to the majority of people living with HIV for whom the treatments of the Berlin and London patients[29,30] (whose non-HIV life-threatening haematological malignancies warranted aggressive, toxic therapies) pose an unacceptable level of risk. Therefore, LRAs must be identified that are highly effective but have minimal side effects. Here, we used two different but highly complementary animal models[31] to show that treatment with AZD5582 had minimal and transient side effects but resulted in significant increases in HIV and SIV RNA levels both in the plasma and in resting $CD4^+$ T cells isolated from all analysed tissues from BLT mice and from the lymph nodes of macaques. Our results provide in vivo evidence of systemic HIV and SIV latency reversal from resting $CD4^+$ T cells. The concordance between the results obtained in two fundamentally different animal models highlights the robust and reproducible nature of the effect of AZD5582 on HIV and SIV reservoirs. The fact that there is little toxicity associated with the use of AZD5582 strongly suggests that activators of the ncNF-κB pathway may be well-suited for HIV eradication approaches in humans.

Online content

Any methods, additional references, Nature Research reporting summaries, source data, extended data, supplementary information, acknowledgements, peer review information; details of author contributions and competing interests; and statements of data and code availability are available at https://doi.org/10.1038/s41586-020-1951-3.

1. Finzi, D. et al. Latent infection of $CD4^+$ T cells provides a mechanism for lifelong persistence of HIV-1, even in patients on effective combination therapy. *Nat. Med.* **5**, 512–517 (1999).
2. Archin, N. M. et al. Interval dosing with the HDAC inhibitor vorinostat effectively reverses HIV latency. *J. Clin. Invest.* **127**, 3126–3135 (2017).
3. Archin, N. M. et al. Administration of vorinostat disrupts HIV-1 latency in patients on antiretroviral therapy. *Nature* **487**, 482–485 (2012).
4. Elliott, J. H. et al. Activation of HIV transcription with short-course vorinostat in HIV-infected patients on suppressive antiretroviral therapy. *PLoS Pathog.* **10**, e1004473 (2014).
5. Gutiérrez, C. et al. Bryostatin-1 for latent virus reactivation in HIV-infected patients on antiretroviral therapy. *AIDS* **30**, 1385–1392 (2016).
6. Kulkosky, J. et al. Intensification and stimulation therapy for human immunodeficiency virus type 1 reservoirs in infected persons receiving virally suppressive highly active antiretroviral therapy. *J. Infect. Dis.* **186**, 1403–1411 (2002).
7. Prins, J. M. et al. Immuno-activation with anti-CD3 and recombinant human IL-2 in HIV-1-infected patients on potent antiretroviral therapy. *AIDS* **13**, 2405–2410 (1999).
8. Rasmussen, T. A. et al. Panobinostat, a histone deacetylase inhibitor, for latent-virus reactivation in HIV-infected patients on suppressive antiretroviral therapy: a phase 1/2, single group, clinical trial. *Lancet HIV* **1**, e13–e21 (2014).
9. Søgaard, O. S. et al. The depsipeptide romidepsin reverses HIV-1 latency in vivo. *PLoS Pathog.* **11**, e1005142 (2015).
10. Ke, R., Conway, J. M., Margolis, D. M. & Perelson, A. S. Determinants of the efficacy of HIV latency-reversing agents and implications for drug and treatment design. *JCI Insight* **3**, e123052 (2018).
11. Sun, S. C. The noncanonical NF-κB pathway. *Immunol. Rev.* **246**, 125–140 (2012).
12. Fulda, S. Molecular pathways: targeting death receptors and Smac mimetics. *Clin. Cancer Res.* **20**, 3915–3920 (2014).
13. Pache, L. et al. BIRC2/cIAP1 is a negative regulator of HIV-1 transcription and can be targeted by Smac mimetics to promote reversal of viral latency. *Cell Host Microbe* **18**, 345–353 (2015).
14. Hennessy, E. J. et al. Discovery of a novel class of dimeric Smac mimetics as potent IAP antagonists resulting in a clinical candidate for the treatment of cancer (AZD5582). *J. Med. Chem.* **56**, 9897–9919 (2013).
15. Honeycutt, J. B. et al. T cells establish and maintain CNS viral infection in HIV-infected humanized mice. *J. Clin. Invest.* **128**, 2862–2876 (2018).
16. Kessing, C. F. et al. In vivo suppression of HIV rebound by didehydro-cortistatin A, a "block-and-lock" strategy for HIV-1 treatment. *Cell Reports* **21**, 600–611 (2017).
17. Tsai, P. et al. In vivo analysis of the effect of panobinostat on cell-associated HIV RNA and DNA levels and latent HIV infection. *Retrovirology* **13**, 36 (2016).
18. Melkus, M. W. et al. Humanized mice mount specific adaptive and innate immune responses to EBV and TSST-1. *Nat. Med.* **12**, 1316–1322 (2006).
19. Choudhary, S. K. et al. Latent HIV-1 infection of resting $CD4^+$ T cells in the humanized $Rag2^{-/-}\ \gamma_c^{-/-}$ mouse. *J. Virol.* **86**, 114–120 (2012).
20. Denton, P. W. et al. Generation of HIV latency in humanized BLT mice. *J. Virol.* **86**, 630–634 (2012).
21. Wahl, A. et al. Precision mouse models with expanded tropism for human pathogens. *Nat. Biotechnol.* **37**, 1163–1173 (2019).
22. Mavigner, M. et al. Simian immunodeficiency virus persistence in cellular and anatomic reservoirs in antiretroviral therapy-suppressed infant rhesus macaques. *J. Virol.* **92**, e00562-18 (2018).
23. Mavigner, M. et al. Pharmacological modulation of the Wnt/β-catenin pathway inhibits proliferation and promotes differentiation of long-lived memory CD4 T cells in antiretroviral therapy-suppressed simian immunodeficiency virus-infected macaques. *J. Virol.* **94**, e01094-19 (2019)
24. Abrahams, M. R. et al. The replication-competent HIV-1 latent reservoir is primarily established near the time of therapy initiation. *Sci. Transl. Med.* **11**, eaaw5589 (2019).
25. Anderson, E. M. & Maldarelli, F. The role of integration and clonal expansion in HIV infection: live long and prosper. *Retrovirology* **15**, 71 (2018).
26. Ferris, A. L. et al. Clonal expansion of SIV-infected cells in macaques on antiretroviral therapy is similar to that of HIV-infected cells in humans. *PLoS Pathog.* **15**, e1007869 (2019).
27. Kuo, H. H. & Lichterfeld, M. Recent progress in understanding HIV reservoirs. *Curr. Opin. HIV AIDS* **13**, 137–142 (2018).
28. Clutton, G. T. & Jones, R. B. Diverse impacts of HIV latency-reversing agents on $CD8^+$ T-cell function: implications for HIV cure. *Front. Immunol.* **9**, 1452 (2018).
29. Gupta, R. K. et al. HIV-1 remission following CCR5Δ32/Δ32 haematopoietic stem-cell transplantation. *Nature* **568**, 244–248 (2019).
30. Hütter, G. et al. Long-term control of HIV by *CCR5* Delta32/Delta32 stem-cell transplantation. *N. Engl. J. Med.* **360**, 692–698 (2009).
31. Nixon, C, C., Mavigner, M., Silvestri G. & Garcia, J. V. In vivo models of human immunodeficiency virus persistence and cure strategies. *J. Infect. Dis.* **215**, S142–S151 (2017).

Methods

Experimental design

The purpose of this study was to determine the efficacy of the SMAC-mimetic AZD5582 as an HIV and SIV LRA in vivo. To this end, two animal models of HIV-1 infection were used: the HIV-infected BLT humanized mouse model and the SIV-infected rhesus macaque (*Macaca mulatta*) nonhuman primate (NHP) model. In each model, animals were infected with HIV-1 or SIV and viraemia was durably suppressed with ART. AZD5582 was administered to infected ART-suppressed animals that were then assessed for changes associated with the reactivation of the viral reservoir. Mice were maintained under specific-pathogen-free conditions by the Division of Comparative Medicine at the University of North Carolina, Chapel Hill. Mouse experiments were conducted in accordance with NIH guidelines for the housing and care of laboratory animals and in accordance with protocols reviewed and approved by the Institutional Animal Care and Use Committee (IACUC) at the University of North Carolina, Chapel Hill. Healthy rhesus macaques for pharmacokinetic studies were housed at GlaxoSmithKline and all procedures were conducted in accordance with the GlaxoSmithKline policy on the care, welfare and treatment of laboratory animals and were reviewed by the IACUC at GlaxoSmithKline. Rhesus macaques infected with SIV were housed at the Yerkes National Primate Research Center and treated in accordance with Emory University and Yerkes National Primate Research Center IACUC regulations (PROTO201800308). Animal-care facilities are accredited by the US Department of Agriculture and the Association for Assessment and Accreditation of Laboratory Animal Care International.

Preparation of Jurkat HIV–luciferase cell clones

Cell clones Jurkat-C16 and Jurkat-I15 were prepared by infecting Jurkat cells (Jurkat clone E6-1 cells, American Type Culture Collection TIB-152, authenticated by morphological identification and virus-susceptibility profiles, tested for mycoplasma by the supplier) with a full-length, infectious HIV-1_{NL4-3}-based virus engineered to express a luciferase reporter in place of the HIV-1 *nef* gene (NLCH-Luci). The Jurkat-N6 cell clone was generated using the same virus as described above with an additional mouse heat-stable antigen (HSA) reporter located just downstream of the luciferase open-reading frame and separated by a T2A element (NLCH-Luci-HSA). NLCH, provided by R. Swanstrom, is the parent molecular infectious clone used to make the Jurkat clones and is a modification of HIV-1_{NL4-3} (GenBank U26942) in which flanking sequences were removed. All viruses were derived by transfection of human embryonic kidney 293 cells (HEK 293T, European Collection of Authenticated Cell Cultures, authenticated by morphological identification, tested for mycoplasma by the supplier) with 1 μg of the HIV-1_{NL4-3}-derived infectious molecular plasmid DNA using the FuGENE HD Transfection reagent (Promega) according to the manufacturer's recommendations. Supernatants were collected 48 h after transfection, passed through a 0.2-μm filter, and used to infect wild-type Jurkat cells. After infection, cells expressing high levels of HIV-encoded mouse HSA were removed using biotin-labelled rat anti-mouse CD24 antibody (clone M1/69, BD Biosciences) that was adsorbed to streptavidin-labelled magnetic Dynabeads M-280 (Life Technologies) according to the manufacturer's recommendations. Negatively selected HIV-infected Jurkat cells were then limit-diluted to 0.5 cells per well in 96-well plates, and individual cell clones were expanded for 2–4 weeks in culture in the presence of 500 nM efavirenz. Clones were profiled for baseline reporter level and responsiveness to benchmark LRAs, with C16, I15 and N6 representing the most quiescent but inducible clones that were obtained.

Cell culture and Jurkat HIV–luciferase assay

Jurkat HIV–luciferase clones were maintained in Roswell Park Memorial Institute (RPMI) 1640 medium (Gibco, Life Technologies) containing 10% (v/v) fetal bovine serum (FBS; SAFC, Sigma-Aldrich), 25 U ml^{-1} penicillin and 25 U ml^{-1} streptomycin (Gibco, Life Technologies), and were split 1:4 every 3–4 days to maintain a cell density of around 0.3–1 million cells per ml. The Jurkat clones were maintained with the addition of 500 nM efavirenz to the medium. Three Jurkat cell clones (C16, I15 and N6), each of which contained one or two integrated HIV proviruses that expressed the luciferase reporter gene, were added at equal amounts for a total of 5,000 cells per well to 384-well plates containing compound titrations. Dose–response testing was performed on compounds dissolved in dimethyl sulfoxide (DMSO; Fisher Scientific) dispensed in duplicate serial threefold, 14-point titrations using a D300e Digital Droplet Dispenser (Hewlett-Packard) to give final assay concentrations ranging from 10 μM to 2.1 pM in 50 μl of medium with a final concentration of 0.5% DMSO (v/v). Cells and compound were incubated at 37 °C for 48 h, unless otherwise indicated, followed by the addition of 20 μl of Steady-Glo Luciferase (Promega). Luminescence resulting from the induction of virally expressed luciferase was measured using an EnVision 2102 Multilabel Plate Reader (Perkin Elmer). Dose–response relationships were analysed with GraphPad Prism (v.6) using a four-parameter logistic regression model to calculate the concentration of compound that provides the half-maximal response and the maximal percentage activation compared to the vehicle control.

Immunoblot analyses

For the immunoblot assays, 10 μg of cell lysate was loaded per well into 4–20% Tris-Glycine SDS–PAGE gels. Proteins from the SDS–PAGE gels were transferred to Turbo Midi PVDF Transfer Packs (BioRad) using the 'Mixed MW' protocol for one Midi Format Gel (constant 2.5 A up to 25 V, for 7 min) of the Trans-Blot Turbo Transfer System (BioRad) with pre-made Trans-Blots according to the manufacturer's instructions. After transfer, PVDF membranes were blocked in 5% bovine serum albumin (BSA) in 1× Tris-buffered saline (TBS) (BioRad) with 0.1% Tween-20 for 1 h at room temperature with gentle rocking. Primary antibodies were added and incubated overnight at 4 °C (anti-cIAP1, 1:1,000 (Abcam); anti-p100/p52, 1:1,000 (Cell Signaling Technology); anti-IκBα, 1:1,000 (Cell Signaling Technology); anti-cIAP2, 1:1,000 (Abcam); and anti-actin-HRP conjugate, 1:30,000 (Abcam). After staining with primary antibodies, the membrane was washed three times with 1× TBS and 0.1% Tween-20, 10 min each wash. After washing, the membrane was incubated in 5% BSA in 1× TBS and 0.1% Tween-20 with the appropriate secondary antibody for 2 h at room temperature. After staining with secondary antibodies, the membrane was washed twice for 10 min with 1× TBS and 0.1% Tween-20 followed by a 10-min wash with 1× TBS. The membrane was then patted dry with filter paper and an image was captured of the undeveloped membrane on a ChemiDoc MP Imaging System using Image Laboratory software (v.6.0.1, BioRad). Sufficient ECL reagent (GE Healthcare) was used to cover the membrane and a series of images was taken with increasing exposure times until the luminescence from the developed membrane saturated the image. The developed membrane was then washed 3 times with 1× TBS for 5 min to remove the residual ECL reagent and then stored at 4 °C in sufficient 1× TBS to submerse the entire membrane. Densitometry of images of the developed membrane was then carried out using Image Laboratory software (v.6.0.1, BioRad). Some membranes were stripped for 1 min with One Minute Plus Western Blot Stripping Buffer (GM Biosciences) and then washed 3 times for 10 min with 1× TBS. The stripped membranes were then blocked in 5% BSA in 1× TBS and 0.1% Tween-20 for 1 h and re-probed overnight with a new primary antibody. To normalize samples for loading a 1:20,000 dilution of β-actin (Abcam) was run on the stripped membranes.

Target gene RT–qPCR

We treated 2 million normal donor $CD4^+$ T cells with a range of concentrations of AZD5582. Total RNA was isolated using the RNEasy Mini kit (Qiagen) according to the manufacturer's instructions. The following

TaqMan primer probe sets were sourced from Applied Biosystems: Hs00985031_g1 (*BIRC3*), Hs00174517_m1 (*NFKB2*) and Hs02800695 (*HPRT1*). TaqMan-based quantitative PCR with reverse transcription (RT–qPCR; Fast Virus 1-Step Master Mix, Applied Biosystems) was used to amplify host genes of interest and acquire the signal on a QuantStudio 3 Real-Time PCR thermocycler (ThermoFisher). Gene expression was normalized to *HPRT1* and the comparative threshold cycle (C_t) method ($\Delta\Delta C_t$) was used for relative quantification of gene expression. Relative quantification was analysed by QuantStudio 3 Real-Time PCR System software (v.1.4.3, ThermoFisher).

HIV quantitative viral outgrowth

All human peripheral-blood mononuclear cell (PBMC) samples were obtained under a specimen procurement protocol reviewed and approved by the University of North Carolina Biomedical Institutional Review Board and the McGill University Health Centre Ethical Review Board. Informed consent was obtained from all participants. Human PBMCs for quantitative viral outgrowth were obtained using continuous flow leukapheresis. Resting $CD4^+$ T cells were isolated and virus outgrowth assays were performed as previously described[32,33] with some modifications. In brief, $20–50 \times 10^6$ highly purified resting $CD4^+$ T cells were stimulated with phytohaemagglutinin, IL-2 (60 U ml^{-1}) and irradiated PBMCs from a seronegative donor, or with 100 nM AZD5582, 335 nM vorinostat or 0.003% DMSO (vehicle control) in limiting dilutions for 24 h. Cultures were washed to remove drugs and $CCR5^{high}$, CD8-depleted, phytohaemagglutinin-stimulated PBMCs from an uninfected donor were added twice to amplify virus outgrowth. Culture supernatants were assayed for HIV p24 expression by ELISA on day 15 and confirmed on day 19. A maximum-likelihood method was used to estimate the frequency of inducible virus and is reported as infectious units per million[34].

RNA-sequencing analysis of human cells

Total $CD4^+$ T cells were isolated from PBMCs of four ART-treated aviraemic patients by negative selection (EasySep Human $CD4^+$ T Cell Enrichment Kit, StemCell) according to the manufacturer's instructions. Dead cells and other debris were removed using a Dead Cell Removal Kit (Miltenyi Biotec) according to the manufacturer's instructions. Cells from each patient were treated with 0.05% DMSO, 100 nM AZD5582 or 25 nM ingenol B and collected 2 h, 6 h and 24 h after exposure. RNA was isolated from the collected cells using AllPrep DNA/RNA Mini Kit (Qiagen). Then, 200 ng of RNA from each sample was checked for quality using an Agilent Bioanalyzer; RNA-integrity number scores were typically >9.0, suggesting that high-quality RNA was obtained. These total RNA samples were then processed into stranded, mRNA libraries using the KAPA library preparation kit (KAPA BioSystems, F. Hoffmann-La Roche). The concentrations of the final libraries were checked by Qubit (Thermo Fisher) and the fragment size distribution (mean size, 359 bp) was analysed with a BioAnalyzer HS-DNA chip (Agilent). Samples were then sequenced using an Illumina Hiseq 4000 sequencer using a paired-end 50-bp by 50-bp run. Samples were successfully demultiplexed and then quality assurance and quality control was carried out using FASTQC (v.0.11.1) (https://www.bioinformatics.babraham.ac.uk/projects/fastqc/).

Raw reads were mapped to the human genome and transcriptome (GRCh38.p7) using STAR[35] and Salmon (v.0.7.2)[36]. Data were normalized and analysed for changes in gene expression using the DESeq2 package[37] in R. *P* values were adjusted for multiple testing using a false-discovery rate using the Benjamini–Hochberg method[38]. Data were analysed both jointly and within each treatment compared with the vehicle control. Differential expression of outliers was assessed and found to have a non-significant overall effect. Thresholds applied to call a significant response were mean $\log_2$-transformed fold change >1 and adjusted $P < 0.05$. Graphs and summary tables were built in R using ggplot. Gene-set enrichment was performed using GSEA (v.2.2.3) and GO analysis (GO PANTHER v.11.1)[39]. Results shown are the mean responses of the four donors tested.

Generation and maintenance of BLT mice

BLT mice were prepared as previously reported[18,40,41]. In brief, a 1–2-mm piece of human liver tissue was sandwiched between two pieces of autologous thymus tissue (Advanced Bioscience Resources) under the kidney capsule of sublethally irradiated (200 cGy) 12–15-week-old female NOD.Cg-*Prkdc*^{scid} *Il2rg*^{tm1Wjl}/SzJ (NSG; The Jackson Laboratory) mice. After implantation, mice were transplanted intravenously with $CD34^+$ haematopoietic stem and progenitor cells isolated from autologous human liver tissue. Human immune cell reconstitution was monitored in the peripheral blood of BLT mice by flow cytometry every 3–4 weeks[21]. For the study that examined the effect of AZD5582 administration on T cell activation, the mean weight of the mice used was 26.88 g and they were approximately 1 year of age at the initiation of the study. For the study that examined the effect of AZD5582 administration on plasma and tissue viraemia during ART suppression, the mean weight of the mice used was 23.14 g and the mice were approximately 7 months old at the initiation of the study. Mice were randomized for assignment to either experimental or control groups (https://www.random.org/).

HIV infection of BLT mice

Stocks of HIV-$1_{JR\text{-}CSF}$ were prepared as follows. The proviral clone was transfected into HEK293T cells using Lipofectamine 2000 (Invitrogen) following the manufacturer's protocols. Viral supernatant was collected 48 h after transfection. Viral supernatant was titrated by infecting TZM-bl cells (NIH AIDS Reagent Program, authenticated by morphological identification and virus-susceptibility profiles, tested for mycoplasma by the supplier) at multiple dilutions. Virus-containing medium was removed the next day and replaced with fresh Dulbecco's modified Eagle medium (DMEM; ThermoFisher) plus 10% FBS and the incubation continued for 24 h. The cells were fixed and stained with 5-bromo-4-chloro-3-indolyl-β-D-galactopyranoside and blue cells were counted directly to determine infectious particles per ml. Each titre of these viral stocks was performed in triplicate and at least two different titre determinations were performed for each virus stock. Exposure of BLT mice to HIV-$1_{JR\text{-}CSF}$ was conducted by tail vein injection with 3×10^4 tissue culture infectious units of virus. Plasma viral load in peripheral blood of infected mice was monitored longitudinally by RT–qPCR using TaqMan RNA to-C_T 1-step kit (Applied Biosystems). The sequences of the forward and reverse primers and the TaqMan probe for PCR amplification and detection of HIV *gag* RNA were: 5′-CATGTTTTCAGCATTATCAGAAGGA-3′, 5′-TGCTTGATGTCCCCCCACT-3′ and 5′-FAM-CCACCCCACAAGATTTAAACACCAT-GCTAA-Q-3′, respectively. For viral load analysis, 40 µl of plasma was collected and analysed with a sensitivity of 350 copies per ml. All samples were run and analysed on an ABI 7500 Fast Real Time PCR System (Applied Biosystems).

SIV infection of NHPs

In total, 21 male and female Indian rhesus macaques, 3–6 years of age, with the exclusion of MamuB*08^+ and MamuB*17^+ macaques, were included in this study (Supplementary Table 7). Rhesus macaques were infected intravenously with 3×10^3 $TCID_{50}$ (50% tissue culture infectious dose) of SIV_{mac239}. The SIV_{mac239} stock was titrated in vitro for viral infectivity by standard end-point titration on CEMx174 cells. The $TCID_{50}$ was calculated as previously described[42]. Standard SIV_{mac239} plasma viral-load quantification was performed regularly throughout the study and three times per week during the AZD5582 treatment period in the Translational Virology Core Laboratory of the Emory Center for AIDS Research using a standard qPCR assay (limit of detection of 60 copies per ml of plasma) as previously described[43]. Ultrasensitive SIV_{mac239} plasma viral-load quantification (limit of detection of 3 copies per ml of plasma) was performed for 2–3 time points before

AZD5582 treatment and 3–4 time points during AZD5582 treatment as previously described[44,45].

ART and AZD5582 treatment of BLT mice and NHPs

ART was administered to BLT mice using irradiated Teklad chow containing emtricitabine (1,500 mg kg^{-1}), tenofovir disoproxil fumarate (1,560 mg kg^{-1}) and raltegravir (600 mg kg^{-1}) (Research Diets). Both the AZD5582 and the vehicle control (10% sterile captisol dissolved in sterile distilled water) were prepared fresh for each administration. AZD5582-2HCl was obtained from ChemieTek and dissolved at 5 mg ml^{-1} in sterile distilled water (Gibco, Life Technologies) containing 10% captisol β-cyclodextrine sulfobutyl ethers sodium salts (Cydex Pharmaceuticals). AZD5582 was administered by intraperitoneal injection at a dose of 3 mg kg^{-1}.

Rhesus macaques were treated with a potent 3-drug ART regimen initiated 56 days after infection that consisted of 2 reverse transcriptase inhibitors, tenofovir disoproxil fumarate (5.1 mg ml^{-1}) and emtricitabine (40 mg ml^{-1}) plus the integrase inhibitor dolutegravir (2.5 mg ml^{-1}). ART was administered once daily at 1 ml kg^{-1} body weight via the subcutaneous route. Peak plasma viral load (measured by the standard assay) and plasma viral load before LRA intervention (as measured by the ultrasensitive assay) were controlled for when allocating macaques into experimental groups. In total, 12 rhesus macaques were treated with AZD5582 and 9 rhesus macaques served as controls. AZD5582 was infused weekly intravenously at 0.1 mg kg^{-1}. Three rhesus macaques received 3 doses of AZD5582 and were euthanized 48 h after the last dose. Nine rhesus macaques received 10 doses of AZD5582 and 3 macaques were euthanized 48 h after the last dose. Among the control rhesus macaques, 4 macaques received a weekly placebo infusion, 2 macaques were euthanized 48 h after 3 infusions and 2 macaques were euthanized 48 h after 10 infusions. The remaining five control macaques received ART only.

Resting $CD4^+$ T cell enrichment

Human resting $CD4^+$ T cells were enriched from total cells isolated from BLT mouse tissues as follows. Each tissue from each mouse was processed individually and then tissues were pooled for immunomagnetic sorting. Each pooled tissue was first enriched for human cells with the EasySep Mouse/Human Chimera Kit (Stem Cell Technologies) and then for resting $CD4^+$ T cells with a human custom selection kit that included the following antibodies: CD8, CD14, CD16, CD19, CD20, CD36, CD56, CD123, glycophorin A, CD66b, CD25 and HLA-DR (all Stem Cell Technologies). Flow cytometry was performed before and after the enrichment to confirm the efficacy of the sort and purity of the sorted samples.

Resting $CD4^+$ T cells from rhesus macaques were isolated from the peripheral blood, bone marrow, lymph node and spleen. Before sorting, $CD4^+$ T cells were enriched using magnetic beads and column purification (Miltenyi Biotec). Enriched $CD4^+$ T cells were then stained with previously determined volumes of the following fluorescently conjugated antibodies: CD3 AF700 (clone SP34-2), CD8 APC-Cy7 (clone SK1), CD69 PE-CF594 (clone FN50), HLA-DR PerCP-Cy5.5 (clone G46-6) (all from BD Bioscience) and CD4 BrilliantViolet (BV)650 (clone OKT4) and CD25 PE-Cy7 (clone BC96) (both from Biolegend). Resting $CD4^+$ T cells were defined as $CD3^+CD4^+CD8^-CD69^-CD25^-HLA\text{-}DR^-$. Sorting was performed on a FACSAria LSR II (BD Biosciences) equipped with FACSDiva software.

Plasma cytokine and chemokine analysis

Human plasma cytokine and chemokine analysis in BLT mice was performed by the University of North Carolina, Chapel Hill Center for AIDS Research Virology Core Laboratory. Plasma was tested undiluted in single wells using a Milliplex MAP kit (Millipore, HCYTMAG-60K-PX41) on a Luminex MAGPIX instrument. The following markers were tested: EGF, eotaxin, FGF-2, FLT-3L, fractalkine, G-CSF, GM-CSF, GRO, IFNα2, IFNγ, IL-1α, IL-1β, IL-1RA, IL-2, IL-3, IL-4, IL-5, IL-6, IL-7, IL-8, IL-9, IL-10, IL-12p40, IL-12p70, IL-13, IL-15, IL-17A, IP-10, MCP-1, MCP-3, MDC, MIP-1α, MIP-1β, PDGF-AA, PDGF-AB/BB, RANTES, sCD40L, TGFα, TNF, TNFβ and VEGF.

Rhesus macaque plasma levels of proinflammatory cytokines and chemokines were evaluated using the NHP MSD V-Plex assay systems developed by MesoScale Discovery. The two validated kits used were the V-PLEX Plus Proinflammatory Panel 1 NHP Kit (K15056D) that evaluates IFNγ, IL-10, IL-1β, IL-2, IL-6 and IL-8, and a custom Chemokine NHP Kit that evaluates IP-10, MCP-1 and MIP-1β (K15055G). The manufacturer-provided protocol was followed with a few modifications. As the plasma samples were infectious, Triton X-100 at a final concentration of 1% was added not only to the subject samples but also to the assay diluents provided with the MSD kit before use. Calibration standards were reconstituted according to the protocol provided with the assay diluent that had the Triton X-100 added to it so that all standards and samples had the same components present. Plasma (60 µl) was diluted twofold with assay diluent and then 50 µl of the diluted sample was added to the assay plate along with 50 µl of the calibrator according the manufacturer's protocol. The plate was then covered and incubated on a shaker for 2 h. After the 2-h incubation, plates were washed at least 6× with the supplied wash buffer and then 25 µl of detection antibodies was added according to the kit protocol. Subsequently, the plate was covered and incubated on a shaker for 2 h at room temperature. After the detection incubation was finished, plates were then washed 6× and 150 µl of 2× read buffer was added to each well and plates were analysed on the Sector s600 MSD plate reader. Data analysis was performed using the MSD Discovery Workbench analysis software.

Cell-associated HIV RNA quantification in BLT mice

For tissue RNA analysis, RNA was extracted using QIAamp viral RNA columns (Qiagen) according to the manufacturer's protocol including an optional treatment with RNase-free DNase and analysed using one-step reverse-transcriptase qPCR (ABI custom TaqMan Assays-by-Design)[46]. Known quantities of HIV *gag* RNA standards were run in parallel, creating a standard curve for HIV *gag* and sample RNA was quantified by extrapolation from the standard curve. All samples were run and analysed on an ABI 7500 Fast Real-Time PCR System (Applied Biosystems). Owing to the relatively low number of human cells found in the brain, HIV RNA levels were quantified for only three vehicle control- and three AZD5582-treated mice.

Immunohistochemical analysis in BLT mice

Tissues for immunohistochemical analysis were collected from BLT mice and fixed in 10% formalin for 16–24 h at 4 °C. Samples were then embedded in paraffin, cut into 5-µm sections and mounted onto poly-L-lysine-coated glass slides. After paraffin removal, antigen retrieval (DIVA Decloaker, Biocare Medical) and blocking of nonspecific immunoglobulin-binding sites (Background Sniper, Biocare Medical), tissue sections were stained with anti-cIAP1 antibody (R&D Systems) overnight at 4 °C. To detect cIAP1, sections were probed with a goat-on-rodent HRP polymer (Biocare Medical) and developed with diaminobenzidine (ImmPact DAB Peroxidase Substrate, Vector Laboratories). As an isotype control, tissue sections were stained with polyclonal goat IgG (R&D Systems) negative control antibodies. Tissue sections were imaged with a Nikon Eclipse Ci microscope using Nikon Elements BR software (v.4.30.01) and a Nikon Digital Sight DS-Fi2 camera.

Serum chemistry analysis in mice

After treatment with AZD5582 for 24 h, serum chemistry analysis in female 20-week-old BALB/cJ mice (The Jackson Laboratory) was performed by the University of North Carolina, Chapel Hill Animal Histopathology Core Laboratory of the Lineberger Comprehensive Cancer Center. All clinical chemistry was performed on an Alfa Wassermann Vet Axcel analyser using Alfa Wassermann reagents. Automated assays for each analyte were as follows and performed according to the

manufacturer's instructions: alkaline phosphatase, Tietz-optimized Bowers and McComb assay; aspartate aminotransferase, Henry modification of Karmen's assay; alanine aminotransferase, Henry modification of Wroblewski and LaDue assay; creatinine, Jaffe reaction; blood urea nitrogen, enzymatic assay; albumin, Doumas and Briggs modification of the bromcresol green dye method; amylase, based on the use of chromogenic 2-chloro-*p*-nitrophenol linked with maltotriose; calcium, calcium-arsenazo assay phosphorus, based on the method of Daly and Ertingshausen with modifications by Armador and Urban; total bilirubin, Walters and Gerarde modification of the DMSO method; total protein, modification of Weichselbaum's biuret reagent.

Immunophenotyping of BLT mice by flow cytometry

Immunophenotyping was performed on peripheral-blood samples collected longitudinally and at study end point, on blood and mononuclear cells isolated from the tissues of BLT mice. All flow cytometry data were collected on either BD LSR Fortessa or BD FACSCanto instruments using BD FACSDiva software (v.6.1.3) and data were analysed with FlowJo software (v.10.4.2). Antibodies used for longitudinal monitoring of human cells in peripheral blood include anti-CD45 APC (clone HI30, BD Biosciences), anti-CD3 FITC (clone HIT3a, BD Biosciences), anti-CD4 PE (clone RPA-T4, BD Biosciences) and anti-CD8 PerCP (clone SK1, BD Biosciences). Flow cytometry gating for the expression of lineage-specific antigens on human leukocytes was performed as follows. Step 1, forward- and side-scatter properties were used to set a live-cell gate. Step 2, live cells were then analysed for expression of the human pan-leukocyte marker CD45. Step 3, human leukocytes were then analysed for human $CD3^+$ T cells. Step 4, T cells were analysed for human CD4 and CD8 expression (Supplementary Fig. 2a).

At collection, peripheral blood and cells isolated from each individual tissue were stained with antibodies to detect human CD45, CD3, CD4, CD8, CD38 (anti-CD38 APC, clone HB7, BD Biosciences) and HLA-DR (anti-HLA-DR PE, clone TU36, BD Biosciences) to assess T cell activation. The following gating strategy was used. Step 1, forward- and side-scatter properties were used to set a live cell gate. Step 2, live cells were then analysed for expression of the human pan-leukocyte marker CD45. Step 3, human leukocytes were subsequently analysed for human $CD3^+$ T cells. Step 4, T cells were analysed for human CD4 and CD8 expression. Step 5, either $CD4^+$ or $CD8^+$ T cells were analysed for the expression of CD38 and HLA-DR (Supplementary Fig. 2b).

To determine the success of the sort and the purity of the sorted human resting $CD4^+$ T cells, the following antibodies were used to analyse pre-sort and post-sort samples: anti-CD3 BV421 (clone UCHT1, BD Biosciences), anti-HLA-DR PerCP (clone L243, BD Biosciences), anti-CD4 BV605 (clone RPA-T4, BD Biosciences), anti-CD8 APC-Cy7 (clone SK1, BD Biosciences), anti-CD25 APC (clone 2A3, BD Biosciences) and anti-CD45 V500 (clone H130, BD Biosciences). Antibodies used as isotype controls: anti-mouse IgG1κ APC (clone MOPC-21, BD Biosciences), anti-mouse IgG2ακ PerCP (clone X39, BD Biosciences), anti-mouse IgG1κ PE (clone MOPC-21, BD Biosciences), anti-mouse IgG1κ PE-Cy7 (clone MOPC-21, BD Biosciences) and anti-mouse IgG2ακ FITC (clone G155-178, BD Biosciences). Flow cytometry gating was performed as follows. Step 1, live cells were gated based on forward scatter and side scatter. Step 2, human haematopoietic cells were gated based on expression of human CD45. Step 3, human T cells were gated based on expression of CD3. Step 4, T cell subsets were gated based on the expression of human CD8 and CD4. Step 5, expression of activation markers (CD25 and HLA-DR) were analysed on the surface of $CD4^+$ T cells (Supplementary Fig. 2c).

NHP sample collection and processing

EDTA-anticoagulated blood samples were collected regularly and used for a complete blood count, routine chemical analysis and immunostaining. Plasma was separated by centrifugation within 1 h of phlebotomy. At the end of the studies, tissue samples were collected, including lymph nodes (21 rhesus macaques), spleen (10 rhesus macaques) and bone marrow (11 rhesus macaques). After 2 washes in RPMI and removal of connective and fat tissues, lymph nodes were ground using a 70-µm cell strainer. PBMCs and bone-marrow mononuclear cells were prepared by density-gradient centrifugation. $CD4^+$ T cells were negatively selected from fresh or frozen cell suspensions using magnetically labelled microbeads and subsequent column purification according to the manufacturer's protocol (Miltenyi Biotec).

AZD5582 pharmacokinetics in NHPs

Three healthy male rhesus macaques of Indian origin (aged 6–7 years, 10.5–13.0 kg) were used for the study. Fasted rhesus macaque received 0.1 mg kg^{-1} of AZD5582 in 10% captisol and ≤5% DMSO (dose volume 0.25 ml kg^{-1} at 0.40 mg ml^{-1}), filtered during administration (0.22-µm PES in-line filter, Millex), via a 30-min saphenous vein infusion (infusion pump, Harvard Apparatus). Blood from femoral venipuncture or saphenous catheters was collected to obtain samples for plasma pharmacokinetics (K2 EDTA microtainers spun at 13,000 rpm for 5 min to obtain plasma), flow cytometry (Cytochex tubes (Streck)) and PBMC isolation (CPT blood collection tubes, BD Biosciences) processed according to the manufacturers' instructions and a dry pellet of cells was snap-frozen on dry ice and stored at −80 °C at various times after administration. AZD5582 was extracted from macaque plasma samples with an isotopically labelled internal standard (rilpivirine-d6) using protein precipitation. The compound was then eluted from a Waters Atlantis T3 (50 mm × 2.1 mm, 3 µm particle size) analytical column under reverse-phase conditions and detected on an AB Sciex API-5000 triple quadrupole mass spectrometer under TurboIonspray mode. Standards were prepared in singlet and quality controls in duplicate, and a calibration curve was generated using a weighted $1/(x^2)$ linear regression of the concentration (x) versus the analyte:internal standard peak area ratio (y). Concentrations of quality controls and study samples were calculated from this calibration curve using Sciex Analyst Software (v.1.6.2). The acceptance criterion of the assay was ±25% of the nominal concentration for standards and quality controls, and the quantifiable range was 2–2,000 ng ml^{-1}.

Ex vivo analysis of AZD5582 activity in NHP cells

Splenocytes from rhesus macaques were initially processed as above and frozen in FBS and 10% DMSO. Cryopreserved splenocytes were thawed and exposed to a range of concentrations of AZD5582 for either 48 h continuously or for 1 h after which the drug was removed by washing and cells were further cultured for 47 h. In preparation for western blot analysis, cells were lysed on ice with intermittent vortex mixing using NP40 Cell Lysis Buffer (Invitrogen, FNN0021) supplemented with appropriately diluted 10× Protease Inhibitor Cocktail (Sigma, P-2714), 1 mM PMSF (Sigma, 93482) and 1 mM DTT (Sigma, 43816) to create a final concentration of 1 mM each in the complete lysis buffer. The lysed cells were then centrifuged at 13,000 rpm for 10 min at 4 °C and then supernatants (soluble fraction lysates) were removed and stored at −80 °C or used immediately for protein concentration and western blot analysis.

Flow cytometry assay for p100 protein

Whole blood collected in Cyto-Chex blood collection tubes (Myriad RBM) was added to ACK lysis buffer to remove red-blood cells, washed with PBS and resuspended in a staining cocktail that included anti-CD3 BV421 (clone SP34-2, BD Biosciences), anti-CD16 BV605 (clone SG8, BD Biosciences), anti-CD4 BV711 (clone L200, BD Biosciences), anti-CD14 BV786 (clone M5E2, BD Biosciences), anti-CD123 PerCP-Cy5.5 (clone 7G3, BD Biosciences), anti-CD20 PE-CF594 (clone 2H7, BD Biosciences), anti-CD8 PE-Cy7 (clone SK1, BD Biosciences), anti-CD11c Alexa700 (clone 3.9, eBioscience) and anti-HLA-DR APC-Cy7 (clone L243, BD Biosciences). After surface-staining, cells were washed twice with PBS, permeabilized using the Cytofix/Cytoperm kit (BD Biosciences, kit used as directed) and stained intracellularly with anti-p100 antibody

(clone EPR18756; Abcam). Cells were washed twice and stained with a secondary chicken anti-rabbit Alexa Fluor 488 antibody (Invitrogen). Samples were acquired using a four-laser Fortessa flow cytometer (BD Biosciences) and analysed with FlowJo software (version 9.7.6, TreeStar).

SIV *env* sequencing and analysis

To generate *env* cDNA, reverse transcription of viral RNA was performed using SuperScript III reverse transcriptase according to the manufacturer's directions (Invitrogen) and the gene-specific primer SIVEnvR1 5′-TGTAATAAATCCCTTCCAGTCCCCCC-3′). Single-genome amplification of SIV *env* was performed by serially diluting this cDNA in independent PCR reactions to identify a dilution in which amplification occurred in <30% of the total number of reactions. PCR amplification was performed with 1× PCR buffer, 2 mM $MgSO_4$, 0.2 mM of each deoxynucleoside triphosphate, 0.2 μM of each primer and 0.025 U μl^{-1} Platinum Taq High Fidelity polymerase (Invitrogen) in a 20-μl reaction. First-round PCR was performed with primer SIVEnvF1 5′-CCTCCCCTCCAGGACTAGC-3′ and antisense primer SIVEnvR1 under the following conditions: 1 cycle of 94 °C for 2 min, 35 cycles at 94 °C for 15 s, 55 °C for 30 s and 68 °C for 5 min, followed by a final extension of 68 °C for 10 min. Next, 1 μl from the first-round PCR product was added to a second-round PCR reaction that included the sense primer SIVEnvF2 5′-TATAATAGACATGGAGACACCCTTGAGGGAGC-3′ and antisense primer SIVEnvR2 5′-ATGAGACATRTCTATTGCCAATTTGTA-3′ performed under the same conditions used for first-round PCR, but with a total of 45 cycles. Correctly sized amplicons were identified by agarose gel electrophoresis and directly sequenced with second-round PCR primers and nine SIV-specific primers using BigDye Terminator technology (Applied Biosystems). To confirm PCR amplification from a single template, chromatograms were manually examined for multiple peaks, indicative of the presence of amplicons that resulted from PCR-generated recombination events, Taq polymerase errors or multiple variant templates. Alignment and phylogenetic trees were implemented in Geneious Prime 2019 (Biomatters) using the Muscle algorithm and the neighbour-joining method with the Tamura–Nei genetic distance model, respectively.

Cell-associated SIV RNA and DNA quantification in NHPs

Cell-associated SIV RNA and DNA were measured simultaneously in resting $CD4^+$ T cells isolated from peripheral blood, spleen, bone marrow and lymph nodes (52,279–500,000 cells) or in total $CD4^+$ T cells isolated from peripheral blood or lymph nodes (100,000–500,000 cells), lysed in RLT+ Buffer (Qiagen), and stored at −80 °C. Nucleic acids were extracted using the AllPrep DNA/RNA mini kit (Qiagen) according to the manufacturer's recommendations with an on-column DNase digestion step. Cell-associated DNA quantification of SIV_{mac239} *gag* DNA was performed on the extracted cell-associated DNA by qPCR using a 5′ nuclease (TaqMan) assay with SIV *gag* primers and normalized to the rhesus macaque albumin gene, as previously described[47]. For cell-associated RNA quantification, RNA was reverse-transcribed using the High Capacity cDNA Reverse Transcription kit (ThermoScientific) and random hexamers. SIV *gag* and the rhesus macaque *CD4* gene were quantified by qPCR of the resultant cDNA using Taqman Universal Mastermix II (ThermoScientific). The CD4 primer and probe sequences were Rh-CD4-F 5′-ACATCGTGGTGCTAGCTTTCCAGA-3′, Rh-CD4-R 5′-AAGTGTAAAGGCGAGTGGGAAGGA-3′ and Rh-CD4-probe 5′-AGGCCTCCAGCACAGTCTATAAGAAAGAGG-3′. The means of two replicate wells were used in all analyses. Samples with undetectable SIV DNA or RNA were assigned a level of 1 copy per million cells or million CD4 RNA copies, respectively, for display purposes.

SIV quantitative viral outgrowth assay

Replication-competent SIV reservoirs were measured by the Viral Reservoir Core Laboratory of the Emory Center for AIDS Research. Latently infected cells were quantified using a limiting dilution culture assay in which $CD4^+$ T cells—enriched from lymph node or spleen cells using magnetic beads and column purification (Miltenyi Biotec)—were co-cultured with CEMx174 cells in fivefold serial dilutions ranging from 5×10^6 cells per well to 4×10^5 cells per well. The cells were cultured in RPMI containing 10% FBS and 100 U ml^{-1} IL-2 (Sigma). The ratio of target cells added was 4:1 for the two highest dilutions. A constant number of 1×10^6 CEMx174 cells was added to all other wells. The cultures were split every 7 days, and fresh medium was added. After 21 days, the growth of virus was detected by RT–qPCR. SIV RNA was isolated from 400 μl of culture supernatant using the Zymo viral RNA isolation kit (Zymo Research). DNase treatment was performed using a RQ1 RNase-free DNase kit (Promega). A one-step RT–qPCR targeting SIV *gag* was performed using an Applied Biosystems 7500 Real Time PCR System (Applied Biosystems) and the Taqman Fast Virus 1-step Master Mix (Thermo Scientific) for qRT–PCR with the following primers and probe: SIVgagFwd 5′-GCAGAGGAGGAAATTACCCAGTAC-3′, SIVgagRev 5′-CAATTTTACCCAGGCATTTAATGTT-3′ and SIVgag probe 5′-6FAM-TGTCCACCTGCCATTAAGCCCGA-3IBFQ-3′. The frequencies of infected cells were determined by the maximum-likelihood method[48] and were expressed as infectious units per million $CD4^+$ T cells.

RNA-sequencing analysis of NHP cells

RNA-sequencing (RNA-seq) analysis was conducted at the Yerkes Nonhuman Primate Genomics Core Laboratory (http://www.yerkes.emory.edu/nhp_genomics_core/). RNA was purified from 50,000 peripheral-blood- or lymph-node-derived $CD4^+$ T cells, which were purified by flow cytometry and lysed in 350 μl of RLT buffer at −80 °C, using Qiagen Micro RNEasy columns, and RNA quality was assessed using an Agilent Bioanalyzer. Then, 2 ng of total RNA was used as input for mRNA amplification using 5′ template switch PCR with the Clontech SMART-seq v4 Ultra Low Input RNA kit according to the manufacturer's instructions. Amplified mRNA was fragmented and appended with dual-indexed bar codes using Illumina NexteraXT DNA library preparation kits. Libraries were validated by capillary electrophoresis on an Agilent 4200 TapeStation, pooled and sequenced on an Illumina HiSeq 3000 using 100-bp single reads at an average depth of 25 million reads.

RNA-seq statistical analyses

RNA-seq data were mapped to the MacaM (v.7.8) assembly of the Indian rhesus macaque genome[49] (available at https://www.unmc.edu/rhesusgenechip/index.htm) and alignment was performed with STAR (v.2.5.2) using the annotation as a splice junction reference. Transcripts were annotated using the MacaM (v.7.8.2) annotation. Transcript abundance was estimated within STAR using the htseq-count algorithm and differential-expression analyses were performed using DESeq2. For significance testing using DESeq2, all of the samples from three- and ten-dose rhesus macaques were grouped together, separately for peripheral blood and lymph nodes, and compared with their pre-treatment samples. Genes determined to be differentially expressed by DESeq2 (adjusted $P < 0.05$ and fold change > ±1.5) were tested for enrichment of molecular pathways using the DAVID database[50] (https://david.ncifcrf.gov/) and by using GSEA with the desktop module (https://www.broadinstitute.org/gsea/). Gene sets for GSEA analysis were selected from the MSigDB database (http://software.broadinstitute.org/gsea/msigdb/index.jsp) and from the previously described 'blood transcriptome modules'[51]. Heat maps, DAVID enrichment bar charts and GSEA enrichment plots were generated with the R (v.3.5.0) package ggplot2. Principal component analysis was performed using Partek Genomics Suite software (v.6.6) using a covariance matrix.

Immunophenotyping of NHPs by flow cytometry

Multicolour flow cytometry analysis was performed on whole blood and lymph-node mononuclear cells using predetermined optimal concentrations of the following fluorescently conjugated monoclonal antibodies: CD3 APC-Cy7 (clone SP34-2), Ki-67 AF700 (clone B56), HLA-DR

PerCP-Cy5.5 (clone G46-6), CCR5 APC (clone 3A9), CCR7 FITC (clone A20), CD45RA PE-Cy7 (clone 5H9) and CD62L PE (clone SK11) (all from BD Biosciences); CD8 BV711 (clone RPA-T8), CD4 BV650 (clone OKT4), CD95 BV605 (clone DX2) and PD-1 BV421 (clone EH12.2H7) (all from Biolegend) and CD28 PE-Cy5.5 (clone CD28.2) (from Beckman Coulter). Flow cytometry acquisition and analysis of samples was performed on at least 100,000 events on an LSRII flow cytometer driven by the FACSDiva software package (BD Biosciences). Analyses of the acquired data were performed using FlowJo software (Tree Star, v.10.0.4).

ELISPOT for SIV-specific IFNγ production in NHPs

IFNγ production was evaluated after the stimulation of PBMCs with SIV_{mac239} Gag and SIV_{mac239} Env peptide pools. The following reagents were obtained through the NIH AIDS Reagent Program, Division of AIDS, NIAID, NIH: SIV_{mac239} Env Peptide Pool and the SIV_{mac239} Gag Peptide Pool. To analyse IFNγ expression, we used the Monkey Elispot kit from MABTECH. The manufacturer's instructions were followed as provided with the exception that concanavalin A (final concentration of 2.5 μg ml^{-1}) was used as the positive control agent. ELISPOT plates were blocked for 30 min with 100 μl of RPMI 1640 supplemented with 10% FBS. PBMCs (4×10^5 per well) were incubated with 1 μg ml^{-1} of DMSO, SIV_{mac239} Gag Peptide Pool or SIV_{mac239} Env Peptide Pool for 18 h before running the assay. For each plate, concavalin A was used for the positive control wells. Samples were run in duplicate.

Intracellular cytokine staining

PBMCs from five ART-suppressed SIV-infected rhesus macaques were thawed. Pre-treatment with AZD5582 was performed for 1 h at 100 nm. After two washes, phorbol 12-myristate 13-acetate (PMA) and ionomycin were added for 1 h at 500 ng ml^{-1} and 10 μg ml^{-1}, respectively. DMSO treatment controls were prepared in parallel. After 1 h, brefeldin-A and Golgi stop solution were added following the manufacturer's recommendations (BD GolgiStop Protein Transport Inhibitor, BD Biosciences). Cells were incubated at 37 °C, 5% CO_2 in R10 for 6–8 h before staining with the following antibodies: CD3 APC-Cy7 (clone SP34-2), CD8 BV711 (clone RPA-T8), CD4 BV650 (clone OKT4) (all from Biolegend), and IFNγ PE (clone B7), TNF AF700 (clone Mab11) and IL-2 BV605 (clone MQ1-17H12) (all from BD Biosciences). Flow cytometry acquisition and analysis of samples was performed on at least 100,000 events using an LSRII flow cytometer driven by the FACSDiva software package (BD Biosciences). Analyses of the acquired data were performed using FlowJo (TreeStar, v.10.0.4) and simplified presentation of incredibly complex evaluations (SPICE, v.6.0)[52] software.

Proliferation assay

PBMCs from five ART-suppressed SIV-infected rhesus macaques were thawed and labelled with CellTrace Violet Proliferation Kit according to the manufacturer instructions (Molecular Probes). Cells were plated in R10 in 96-well round-bottom plates at 4 million cells per ml. Pre-treatment with AZD5582 was performed for 1 h at 100 nM. After two washes, PMA and ionomycin were added for 1 h at 500 ng ml^{-1} and 10 μg ml^{-1}, respectively. DMSO treatment controls were prepared in parallel. Cells were incubated at 37 °C, 5% CO_2 in R10 supplemented with 20 IU ml^{-1} IL-2. After 5 days, cells were stained with CD3 APC-Cy7 (clone SP34-2), CD8 BV711 (clone RPA-T8), CD4 BV650 (clone OKT4) (all from Biolegend) and analysed by flow cytometry on an LSRII instrument. Data were analysed using FlowJo software (TreeStar, v.10.0.4).

Statistical analysis

Statistical analyses were performed using GraphPad Prism Software (v.6 or v.7). $P \leq 0.05$ was considered statistically significant. At least three samples were used for each group, the minimum to achieve statistical significance. No statistical methods were used to predetermine sample size. Investigators were not blinded to group allocations or when assessing outcomes. In some instances, cells were pooled from individual humanized mice for each tissue and experimental group for the isolation of resting $CD4^+$ T cells (Fig. 2d and Extended Data Fig. 2). To test the statistical significance of the differences that we observed in PCR data in BLT mouse brains in Fig. 2e and grouped tissue PCR data in Fig. 2d, unpaired two-sided Student's *t*-tests were used. To test the statistical significance of the differences that we observed in PCR data in PBMCs and female reproductive tract in Fig. 2e, T cell activation markers in Supplementary Table 5 and plasma cytokines and chemokines in Supplementary Table 6, we used unpaired two-sided Mann–Whitney *U*-tests. To assess the statistical significance of the differences observed over time in serum enzymes in Supplementary Table 4, we used paired nonparametric Wilcoxon matched-pairs signed-rank tests. To test the statistical significance of the differences in activation marker levels expressed on T cells from rhesus macaques in Fig. 4d, e, as well as the ultrasensitive plasma viral load results in Extended Data Fig. 8b and the ex vivo proliferation assay in Extended Data Fig. 10g, we used Wilcoxon matched-pairs signed-rank tests. To assess the statistical significance of the differences observed between SIV DNA and SIV RNA levels in resting or total $CD4^+$ T cells from rhesus macaques in Fig. 3e and Extended Data Fig. 6b, respectively, as well as for the quantitative viral outgrowth results in Extended Data Fig. 6c, we used unpaired two-sided Mann–Whitney *U*-tests. Unpaired two-sided Mann–Whitney *U*-tests were also used to compare rhesus macaques with stable compared with increased viraemia in Extended Data Fig. 8c.

Reporting summary

Further information on research design is available in the Nature Research Reporting Summary linked to this paper.

Data availability

Source Data for Figs. 1–4, Extended Data Figs. 1, 2, 4, 6–10 and Supplementary Tables 4–6 are provided with the paper. Gene-expression data are available at the Gene Expression Omnibus (GEO) repository (accession number GSE141546 and GSE142774). Any other data are available from corresponding authors on reasonable request.

32. Archin, N. M. et al. Expression of latent HIV induced by the potent HDAC inhibitor suberoylanilide hydroxamic acid. *AIDS Res. Hum. Retroviruses* **25**, 207–212 (2009).
33. Keedy, K. S. et al. A limited group of class I histone deacetylases acts to repress human immunodeficiency virus type 1 expression. *J. Virol.* **83**, 4749–4756 (2009).
34. Trumble, I. M. et al. SLDAssay: a software package and web tool for analyzing limiting dilution assays. *J. Immunol. Methods* **450**, 10–16 (2017).
35. Dobin, A. et al. STAR: ultrafast universal RNA-seq aligner. *Bioinformatics* **29**, 15–21 (2013).
36. Patro, R., Duggal, G., Love, M. I., Irizarry, R. A. & Kingsford, C. Salmon provides fast and bias-aware quantification of transcript expression. *Nat. Methods* **14**, 417–419 (2017).
37. Love, M. I., Huber, W. & Anders, S. Moderated estimation of fold change and dispersion for RNA-seq data with DESeq2. *Genome Biol.* **15**, 550 (2014).
38. Benjamini, Y. & Hochberg, Y. Controlling the false discovery rate: a practical and powerful approach to multiple testing. *J. R. Stat. Soc. B* **57**, 289–300 (1995).
39. Subramanian, A. et al. Gene set enrichment analysis: a knowledge-based approach for interpreting genome-wide expression profiles. *Proc. Natl Acad. Sci. USA* **102**, 15545–15550 (2005).
40. Denton, P. W. et al. Antiretroviral pre-exposure prophylaxis prevents vaginal transmission of HIV-1 in humanized BLT mice. *PLoS Med.* **5**, e16 (2008).
41. Denton, P. W. et al. One percent tenofovir applied topically to humanized BLT mice and used according to the CAPRISA 004 experimental design demonstrates partial protection from vaginal HIV infection, validating the BLT model for evaluation of new microbicide candidates. *J. Virol.* **85**, 7582–7593 (2011).
42. Reed, L. J. & Muench, H. A simple method of estimating fifty per cent endpoints. *Am. J. Epidemiol.* **27**, 493–497 (1938).
43. Palesch, D. et al. Short-term pegylated interferon α2a treatment does not significantly reduce the viral reservoir of simian immunodeficiency virus-infected, antiretroviral therapy-treated rhesus macaques. *J. Virol.* **92**, e00279-18 (2018).
44. Hansen, S. G. et al. Addendum: immune clearance of highly pathogenic SIV infection. *Nature* **547**, 123–124 (2017).
45. Li, H. et al. Envelope residue 375 substitutions in simian–human immunodeficiency viruses enhance CD4 binding and replication in rhesus macaques. *Proc. Natl Acad. Sci. USA* **113**, E3413–E3422 (2016).
46. Krisko, J. F., Martinez-Torres, F., Foster, J. L. & Garcia, J. V. HIV restriction by APOBEC3 in humanized mice. *PLoS Pathog.* **9**, e1003242 (2013).
47. Cartwright, E. K. et al. $CD8^+$ lymphocytes are required for maintaining viral suppression in SIV-infected macaques treated with short-term antiretroviral therapy. *Immunity* **45**, 656–668 (2016).

48. Rosenbloom, D. I. S., Hill, A. L., Laskey, S. B. & Siliciano, R. F. Re-evaluating evolution in the HIV reservoir. *Nature* **551**, E6–E9 (2017).
49. Zimin, A. V. et al. A new rhesus macaque assembly and annotation for next-generation sequencing analyses. *Biol. Direct* **9**, 20 (2014).
50. Huang, W., Sherman, B. T. & Lempicki, R. A. Systematic and integrative analysis of large gene lists using DAVID bioinformatics resources. *Nat. Protocols* **4**, 44–57 (2009).
51. Li, J. et al. Isolation and transcriptome analyses of human erythroid progenitors: BFU-E and CFU-E. *Blood* **124**, 3636–3645 (2014).
52. Roederer, M., Nozzi, J. L. & Nason, M. C. SPICE: Exploration and analysis of post cytometric complex multivariate datasets. *Cytometry* **79A**, 167–174 (2014).

Acknowledgements We thank Garcia and Chahroudi laboratory members, the Animal Histopathology & Laboratory Medicine Core at the University of North Carolina-Chapel Hill (UNC-CH), which is supported in part by an NCI Center Core Support Grant (5P30CA016086-41) to the UNC Lineberger Comprehensive Cancer Center and technicians from the Department of Comparative Medicine at UNC-CH; the HIV/STD Laboratory Core and the Clinical Pharmacology and Analytical Chemistry Core of the UNC Center for AIDS Research (CFAR) (P30 AI050410); D. Hazuda, B. Howell and S. Barrett (Merck & Co.) for assistance with ART-containing chow; Yerkes Animal and Research Resources; the Children's Healthcare of Atlanta and Emory University Pediatric Flow Cytometry Core, Emory CFAR Translational Virology and Reservoir Cores, the Quantitative Molecular Diagnostics Core of the AIDS and Cancer Virus Program, Frederick National Laboratory, as well as GSK for tenofovir disoproxil fumarate, emtricitabine and dolutegravir. This work was supported by the National Institutes of Allergy and Infectious Diseases (NIAID)(AI123010, AI096113, AI111899, AI117851 and P30 AI050410), and Mental Health (NIMH) (MH108179). This work was supported by the Emory Consortium for Innovative AIDS Research in Nonhuman Primates (UM1 AI124436), amfAR (109353-59-RGRL), the Yerkes National Primate Research Center (P51 OD011132) and the Translational Virology and Reservoir Cores of the Center for AIDS Research at Emory University (P30 AI050409). Research was also supported by Qura Therapeutics and by CARE, a Martin Delaney Collaboratory (1UM1AI126619-01) of the NIAID, NINDS, NIDA and NIMH. By the Natural Science Foundation of Guangdong Province, China (2016A030310108), UNC-South China STD Research Training Center (1D43TW009532) and Chinese National Key Technologies R&D Program for the 13th Five-year Plan (2017ZX10202101003). Federal funds were used for this research from the National Cancer Institute, NIH (contracts HHSN261200800001E and 75N91019D0002). The content of this publication does not necessarily reflect the views or policies of the Department of Health and Human Services, nor does mention of trade names, commercial products or organizations imply endorsement by the US Government.

Author contributions J.V.G., A.C., G.S., R.M.D., A.W. and D.M.M. conceived and designed the studies. G.C.S., D.M.I., S.R.W., S.D.F., C.G., E.P.B. and R.G.F. assessed in vitro AZD5582 activity. M.K., Z.W., J.H.B., D.F. and C.D.J. performed the in vitro transcriptomic study. D.F. and J.-P.R. contributed clinical specimens. C.C.N., P.T.H., C.D., N.J.S. and B.L. performed mouse experiments. R.A.S. and C.G.C. performed the qPCR analysis of HIV RNA levels in mouse samples. R.A.C. performed the immunohistochemical analysis. N.M.A. isolated human resting $CD4^+$ T cells. C.C.N. analysed mouse data. M.M., A.D.B. and S.J. performed the monkey experiments. G.C.S., J.D., S.M. and R.M.D. conducted pharmacokinetic studies in NHP. C.M. and N.S. isolated resting $CD4^+$ T cells from macaques. T.H.V. supervised the qPCR analyses of SIV RNA and DNA levels in monkey samples. M.M. and A.D.B. performed flow cytometry and analysed monkey data. G.K.T., A.A.U. and H.W. performed the macaque RNA-seq analyses and S.E.B. analysed these data. C.M.F. and B.F.K. performed *env* sequencing analyses. J.D.L. supervised the ultrasensitive plasma viral loads. G.C.S. and C.G. analysed AZD5582 target engagement in human, mouse and macaque samples and J.D. and R.M.D. analysed the data. C.G. performed the ELISPOTs. C.C.N., M.M., A.W., A.C. and J.V.G. wrote the manuscript with input from all authors.

Competing interests The authors declare no competing interests.

Additional information

Supplementary information is available for this paper at https://doi.org/10.1038/s41586-020-1951-3.

Correspondence and requests for materials should be addressed to R.M.D., A.C. or J.V.G.

Peer review information *Nature* thanks Mathias Lichterfeld and the other, anonymous, reviewer(s) for their contribution to the peer review of this work.

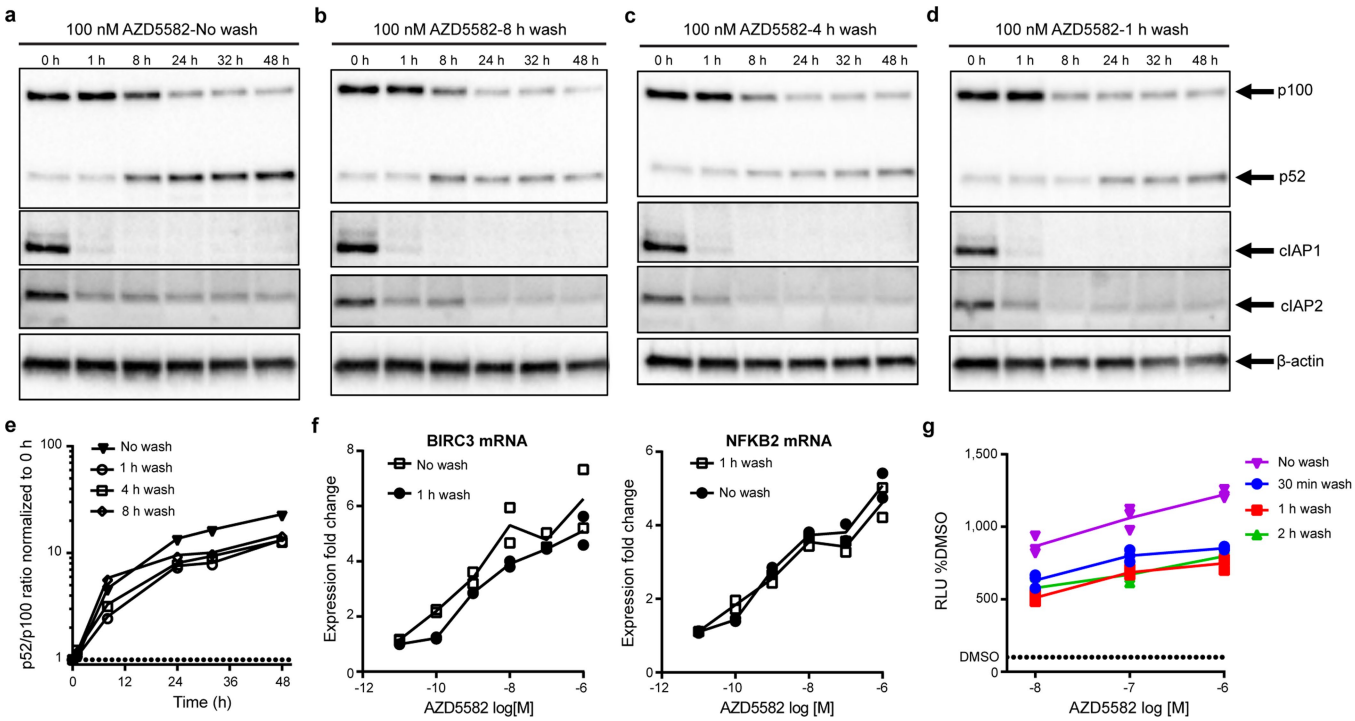

Extended Data Fig. 1 | Short-duration exposure to AZD5582 activates the ncNF-κB pathway. a–**d**, Isolated total human CD4$^+$ T cells treated with 100 nM AZD5582 and then either not washed (**a**) or washed three times with PBS 8 h (**b**), 4 h (**c**) or 1 h (**d**) after treatment. Whole-cell lysates were then analysed by immunoblot for components of the ncNF-κB pathway. **e**, Densitometry analysis of the ratio of p52 to p100 from the pulse-wash assay immunoblots. Points represent values for the densitometric ratio from one western blot, representative of several independent experiments. **a**–**e**, Entire set representative of 1 experiment with 5 replicates of the 1-h wash condition conducted. **f**, Fold induction of ncNF-κB target gene expression in isolated CD4$^+$ T cells from an uninfected donor treated with the indicated concentrations of AZD5582 and either washed after 1 h or not washed, and subsequently cultured for 24 h as measured by RT–qPCR. Points represent two technical replicates and lines represent the mean. The data presented are representative of three independent experiments. **g**, DMSO-normalized induction of luciferase activity from the Jurkat reporter model after exposure to AZD5582 (10, 100 or 1,000 nM) for 30 min (blue), 1 h (red), 2 h (green) or continued exposure (purple). Points represent three replicates in one assay run, representative of two independent experiments. Lines represent the mean of the three replicates. For gel source data, see Supplementary Fig. 1.

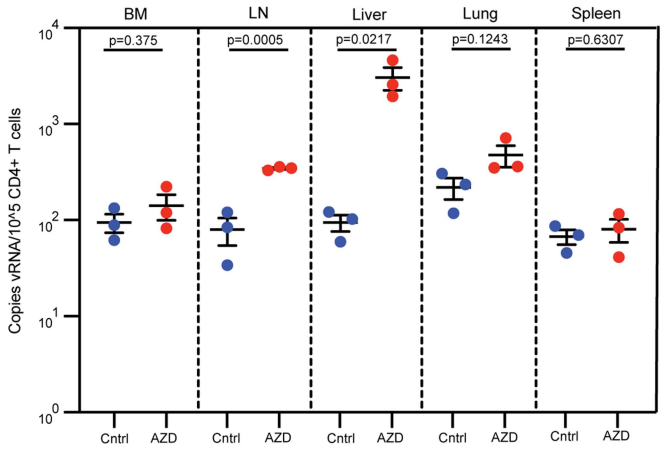

Extended Data Fig. 2 | AZD5582 induces HIV RNA expression in resting CD4$^+$ T cells from tissues of HIV-infected, ART-suppressed BLT mice. HIV RNA levels in resting CD4$^+$ T cells isolated from the bone marrow, lymph nodes, liver, lung and spleen of control (Cntrl, blue circles) or AZD5582-treated (AZD, red circles) mice (cells pooled from $n = 6$ mice per group for each tissue) were analysed in triplicate. Statistical significance was determined with a two-sided Student's *t*-test. The mean fold increase in viral RNA levels in resting CD4$^+$ T cells from tissues in the experiment shown in Fig. 2 was 12.1 (±3.7), whereas in this figure it was 8.4 (±6.0). These values were not statistically different ($P = 0.4286$, two-sided Mann–Whitney *U*-test). Data are mean ± s.e.m.

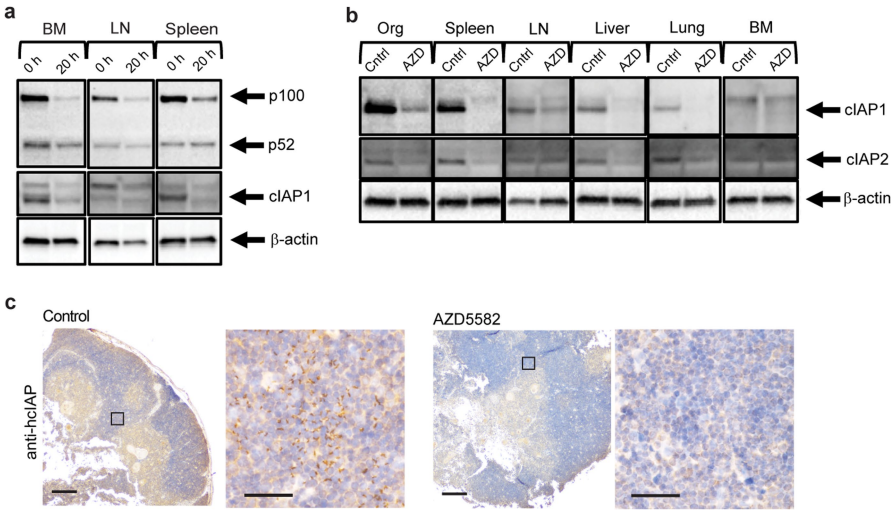

Extended Data Fig. 3 | AZD5582 ex vivo target engagement. a, Western blot analysis of p100, p52 and cIAP1 protein levels in cells isolated from the bone marrow, lymph node and spleen of BLT mice before and 20 h after ex vivo treatment with AZD5582. Loading control, β-actin. Representative of two experiments. **b**, cIAP expression in resting $CD4^+$ T cells isolated from the thymus, spleen, lymph nodes, liver, lung and bone marrow. Loading control, β-actin. Representative of two experiments. **c**, cIAP expression in the thymic organoid of HIV-infected ART-suppressed BLT mice 48 h after the administration of vehicle control or AZD5582 (three control and one AZD5582-treated analysed). Positive cells, brown. Imaged at 4× and 40× magnifications; scale bars, 100 µm (4×) and 50 µm (40×). Boxes in the 4× images indicate regions corresponding to images at 40× magnification. For gel source data, see Supplementary Fig. 1.

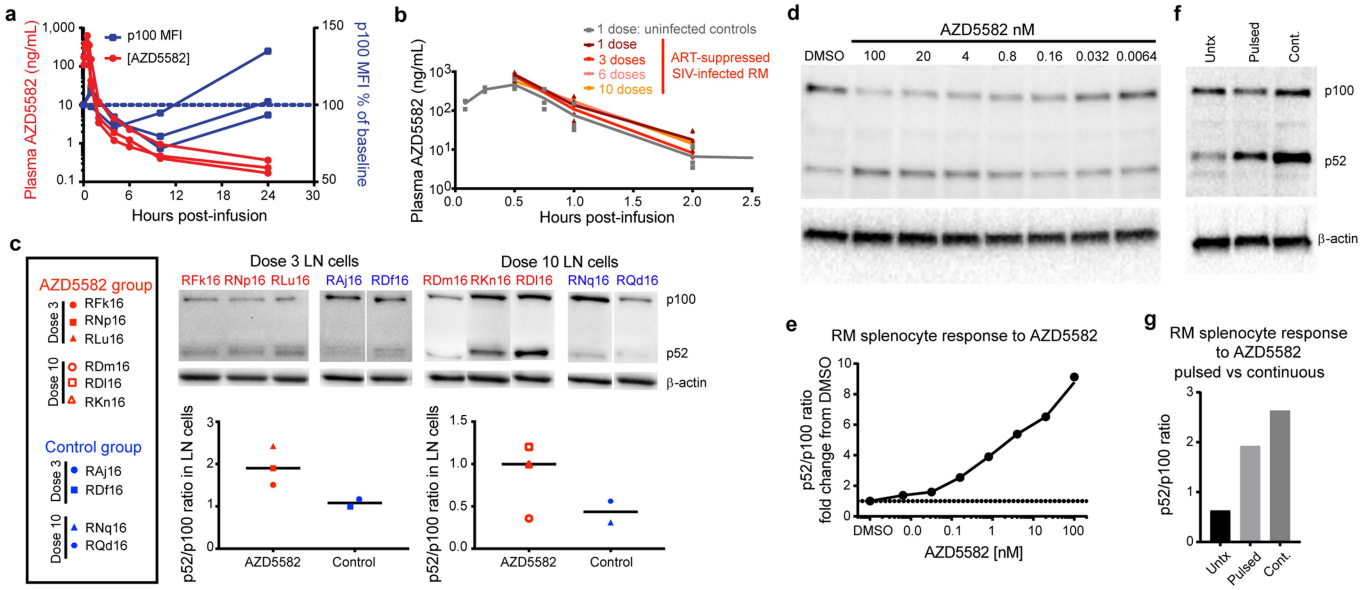

Extended Data Fig. 4 | Pharmacokinetic and pharmacodynamic assessment of AZD5582 in rhesus macaques. a, AZD5582 (0.1 mg kg^{-1}) was administered to healthy rhesus macaques ($n = 3$) by intravenous infusion. Plasma concentrations of AZD5582 (left *y* axis) are shown for the indicated time points. Flow cytometry was used to measure intracellular p100 levels, shown as the geometric mean fluorescence intensity (gMFI) in CD4$^+$ T cells and plotted as the percentage of baseline of p100 gMFI (right *y* axis). **b**, Plasma concentrations of AZD5582 after one (dark red), three (red), six (pink) or ten (orange) doses in six SIV-infected ART-treated rhesus macaques (RM) and after one dose in three uninfected control rhesus macaques (grey). Individual values are shown as symbols. **c**, Western blot analyses of inactive p100 and active p52 forms of NF-κB2 in lymph-node mononuclear cells collected 48 h after the third or tenth dose of AZD5582 in SIV-infected ART-suppressed rhesus macaques (red; $n = 3$ for both the 3-dose and 10-dose groups) or at equivalent time points for placebo controls (blue; $n = 2$ for both the 3-dose and 10-dose groups). Immunoblots are shown in the top panels and densitometry analyses of the p52:p100 ratios are shown in the bottom panels. The line represents the median. **d**, Cryopreserved control rhesus macaque splenocytes were treated with the indicated concentrations of AZD5582 for 48 h, then p100/p52 levels were analysed by western blotting to measure engagement of the ncNF-κB pathway. **e**, DMSO-normalized densitometric p52:p100 ratio versus the AZD5582 concentration. For **d**, **e**, the experiments were performed in duplicate. **f**, Cryopreserved rhesus macaque splenocytes were exposed to DMSO alone (Untx), 100 nM AZD5582 washed off after 1 h and cultured for 47 h (Pulsed) or continuous 100 nM AZD5582 for 48 h (Cont.), after which the cells were studied by western blot for p100 and p52 levels. **g**, Densitometric p52:p100 ratio. For **f**, **g**, data represent a single experiment. For gel source data, see Supplementary Fig. 1.

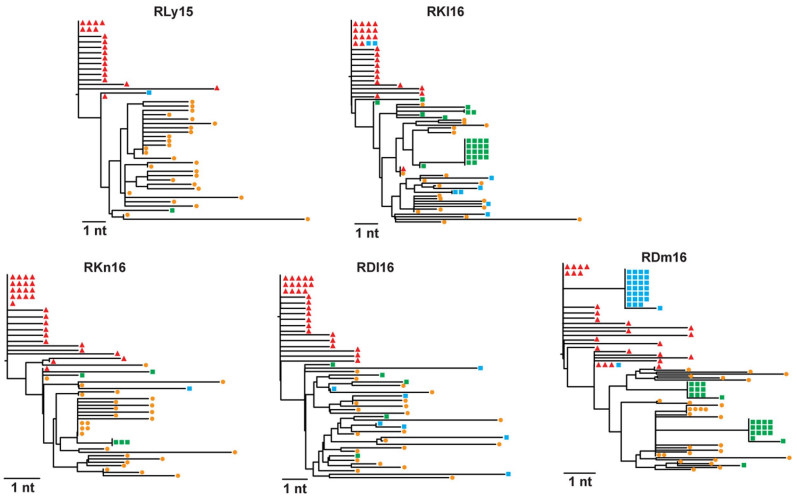

Extended Data Fig. 5 | Phylogenetic trees based on full *env* sequencing. Plasma virus was sequenced from four time points per macaque ($n = 5$): near peak viraemia (2 weeks after infection; red), immediately before ART (8 weeks after infection; orange) and two time points of on-ART viraemia during AZD5582 treatment (green and blue). All sequences per macaque were phylogenetically analysed and the resulting phylogenetic trees are shown for each macaque. The horizontal bar indicates the genetic distance. nt, nucleotide.

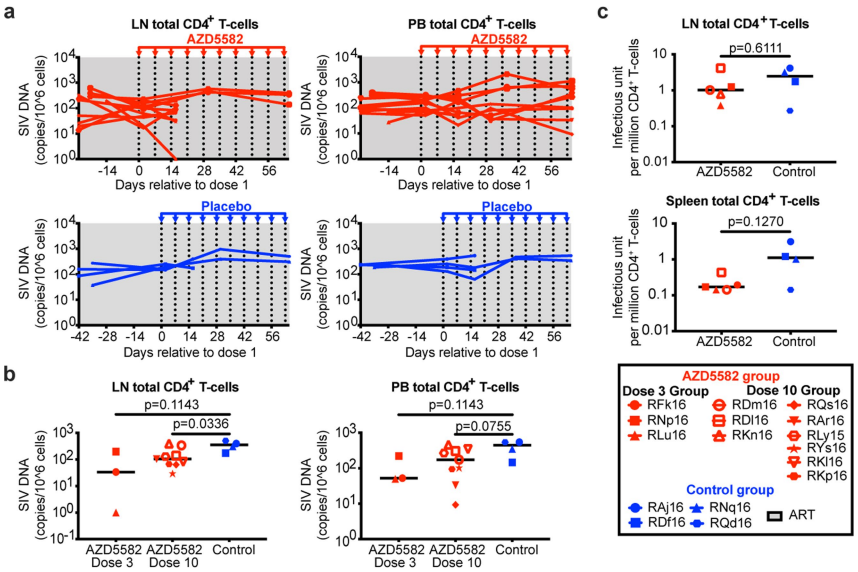

Extended Data Fig. 6 | SIV DNA levels in total CD4$^+$ T cells and replication-competent reservoir size in ART-suppressed SIV-infected rhesus macaques. **a**, Longitudinal assessment of cell-associated SIV DNA levels in total CD4$^+$ T cells isolated from peripheral blood and lymph nodes of AZD5582-treated ($n = 12$, red) and control ($n = 4$, blue) ART-suppressed SIV-infected rhesus macaques. Grey shading represents the period of ART administration. **b**, Comparison of cell-associated SIV DNA levels in total CD4$^+$ T cells isolated from the lymph nodes and peripheral blood of AZD5582-treated and control ART-suppressed SIV-infected rhesus macaques. Total CD4$^+$ T cells were analysed from AZD5582-treated rhesus macaques 48 h after receiving 3 doses (lymph nodes and peripheral blood, $n = 3$) or 10 doses (lymph nodes and peripheral blood, $n = 9$) of AZD5582. Total CD4$^+$ T cells were analysed from placebo-control rhesus macaques (lymph nodes and peripheral blood, $n = 4$) at equivalent time points. Open symbols indicate AZD5582-treated rhesus macaques with on-ART viraemia above 60 copies per ml of plasma. Statistical significance was determined using a two-sided Mann–Whitney *U*-test. **c**, Quantitative viral outgrowth assays were performed for AZD5582-treated rhesus macaques 48 h after receiving 3 doses (lymph nodes, $n = 2$; spleen, $n = 3$) or 10 doses (lymph nodes, $n = 3$; spleen, $n = 2$) of AZD5582. Quantitative viral outgrowth assays were performed from control rhesus macaques (lymph nodes and spleen, $n = 4$) at equivalent time points. Open symbols indicate AZD5582-treated rhesus macaques with on-ART viraemia. Statistical significance was determined with a two-sided Mann–Whitney *U*-test. Horizontal lines represent the median (**b**, **c**).

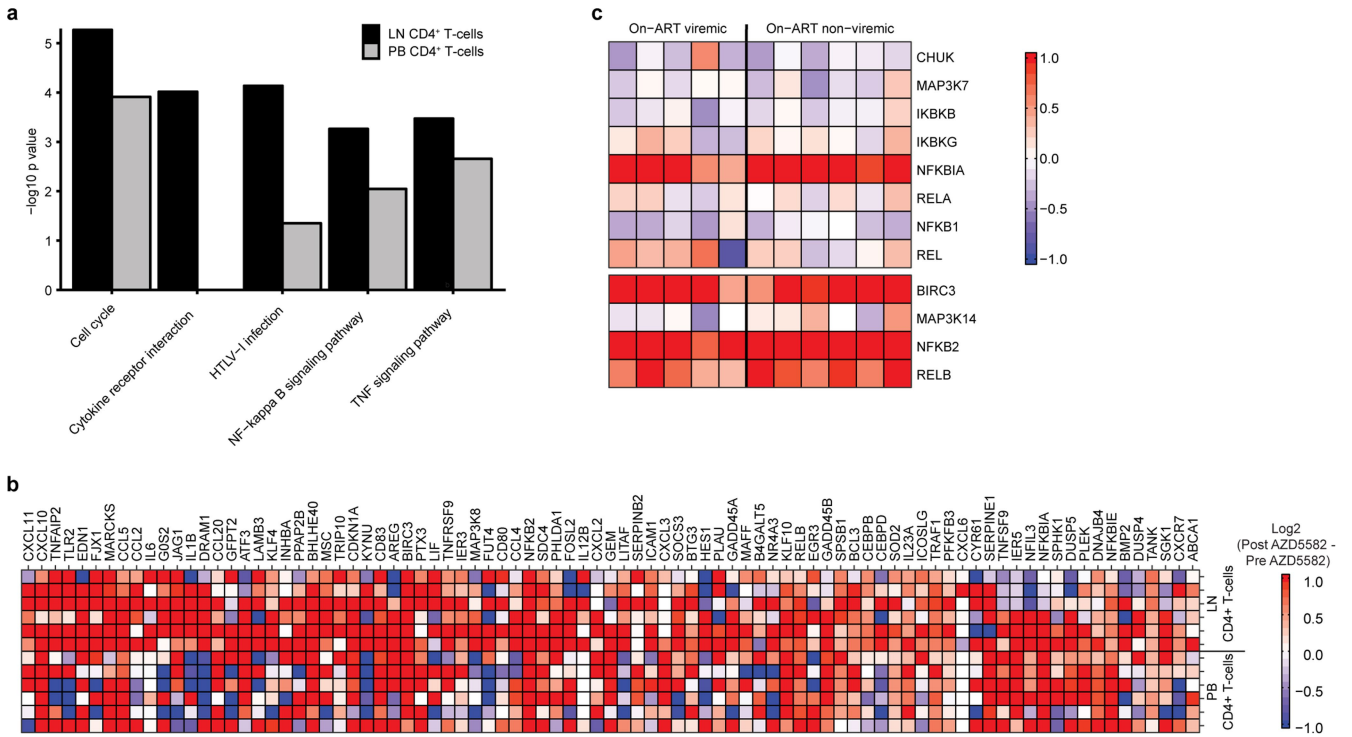

Extended Data Fig. 7 | AZD5582-induced gene pathways and genes in SIV-infected ART-suppressed rhesus macaques. a, DAVID analysis showing pathways significantly enriched in genes differentially expressed after AZD5582 treatment relative to baseline in CD4$^+$ T cells isolated from lymph nodes (black bars) and peripheral blood (grey bars). $n = 6$ for both lymph nodes and peripheral blood; for each, $n = 3$ for 3 doses of AZD5582 and $n = 3$ for 10 doses of AZD5582. **b**, Leading edge genes from the 'hallmark TNF signalling via NF-κB' pathway from MSigDB. Genes were identified in the leading edge of CD4$^+$ T cell samples from the lymph nodes before and after treatment with AZD5582 (shown in Fig. 4b). The contrast depicted is the fold change of each gene for each rhesus macaque's post-treatment sample relative to the pre-treatment values for CD4$^+$ T cells from the lymph nodes (top) and the peripheral blood (bottom). $n = 6$ for both lymph nodes and peripheral blood; for each, $n = 3$ for 3 doses of AZD5582 and $n = 3$ for 10 doses of AZD5582. **c**, Heat map of cNF-κB (top) and ncNF-κB (bottom) pathway gene expression in rhesus macaques with (left, $n = 5$) or without (right, $n = 6$) on-ART viraemia of >60 copies per ml plasma. One rhesus macaque without on-ART viraemia was excluded from this analysis because of technical issues (higher than expected unmapped and multi-mapped reads, and lower than expected unique identified reads compared to the means). Colour scale, $\log_2$-transformed fold changes of post-treatment compared with pre-treatment values.

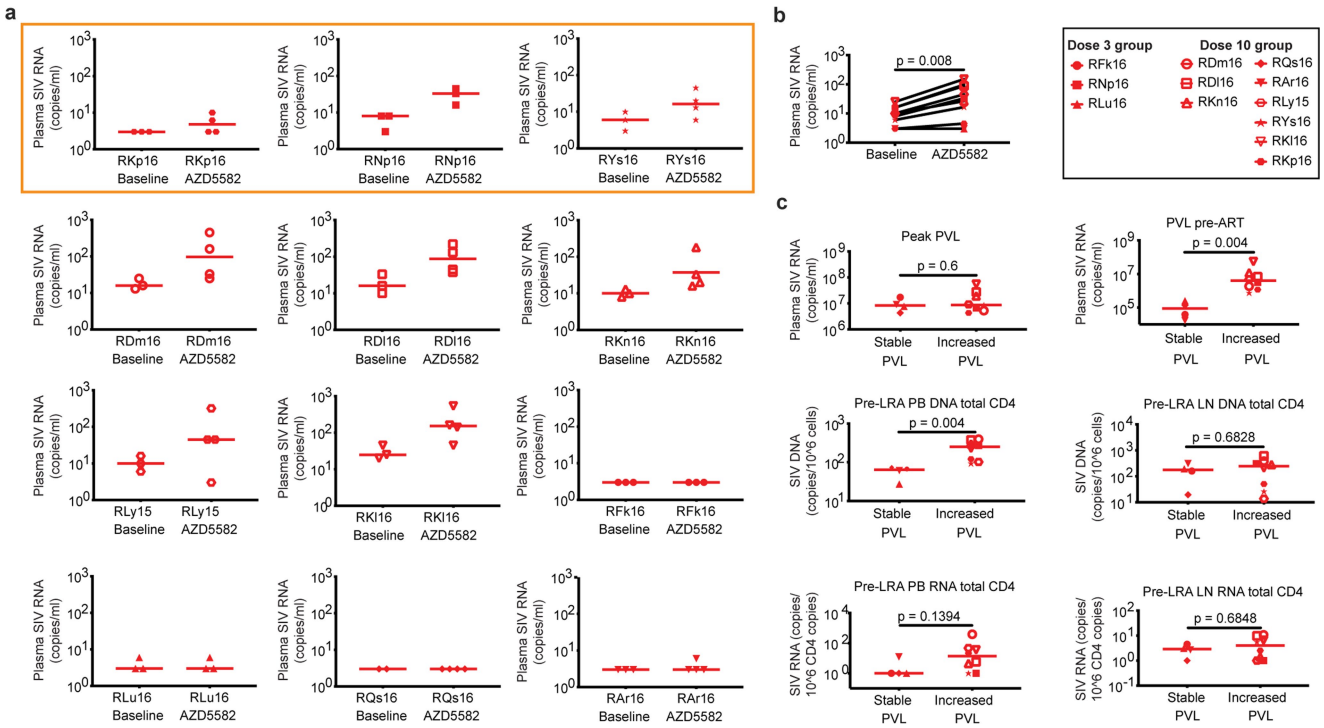

Extended Data Fig. 8 | Relationship between virological status before intervention and virological response to AZD5582 treatment in SIV-infected ART-suppressed rhesus macaques. a, Individual representations of plasma SIV RNA levels measured by ultrasensitive assay (limit of detection 3 copies per ml of plasma) before and during AZD5582 treatment in SIV-infected ART-suppressed rhesus macaques ($n = 12$). 'Baseline' shows two or three plasma viral loads before AZD5582 treatment and 'AZD5582' shows three or four plasma viral loads during AZD5582 treatment. Open symbols indicate the five AZD5582-treated rhesus macaques with on-ART viraemia of >60 copies of SIV RNA per ml of plasma using the standard viral load assay (confirmed with ultrasensitive assay). The orange box highlights an additional 3 rhesus macaques who did not experience on-ART viraemia of >60 copies per ml of plasma but had ≥2 SIV RNA measurements above baseline values using the ultrasensitive quantification method. **b**, Comparison of the medians of plasma SIV RNA levels at baseline and during AZD5582 treatment measured by ultrasensitive assay for ART-suppressed SIV-infected rhesus macaques ($n = 12$). Statistical significance was determined with a Wilcoxon matched-pairs signed-rank test. **c**, Comparison of the levels of plasma SIV RNA at peak, plasma SIV RNA before ART initiation, SIV DNA in peripheral-blood $CD4^+$ T cells before AZD5582 treatment (pre-LRA), SIV DNA in lymph-node $CD4^+$ T cells pre-LRA, SIV RNA in peripheral blood $CD4^+$ T cells pre-LRA and SIV RNA in lymph-node $CD4^+$ T cells pre-LRA in rhesus macaques with increased plasma viral loads (PVL) by standard and/or ultrasensitive assay during AZD5582 treatment (increased plasma viral loads, $n = 8$) compared with rhesus macaques that did not demonstrate increased viral loads (stable plasma viral loads, $n = 4$). Statistical significance was determined using a two-sided Mann–Whitney *U*-test. Horizontal lines represent the median (**a**, **c**).

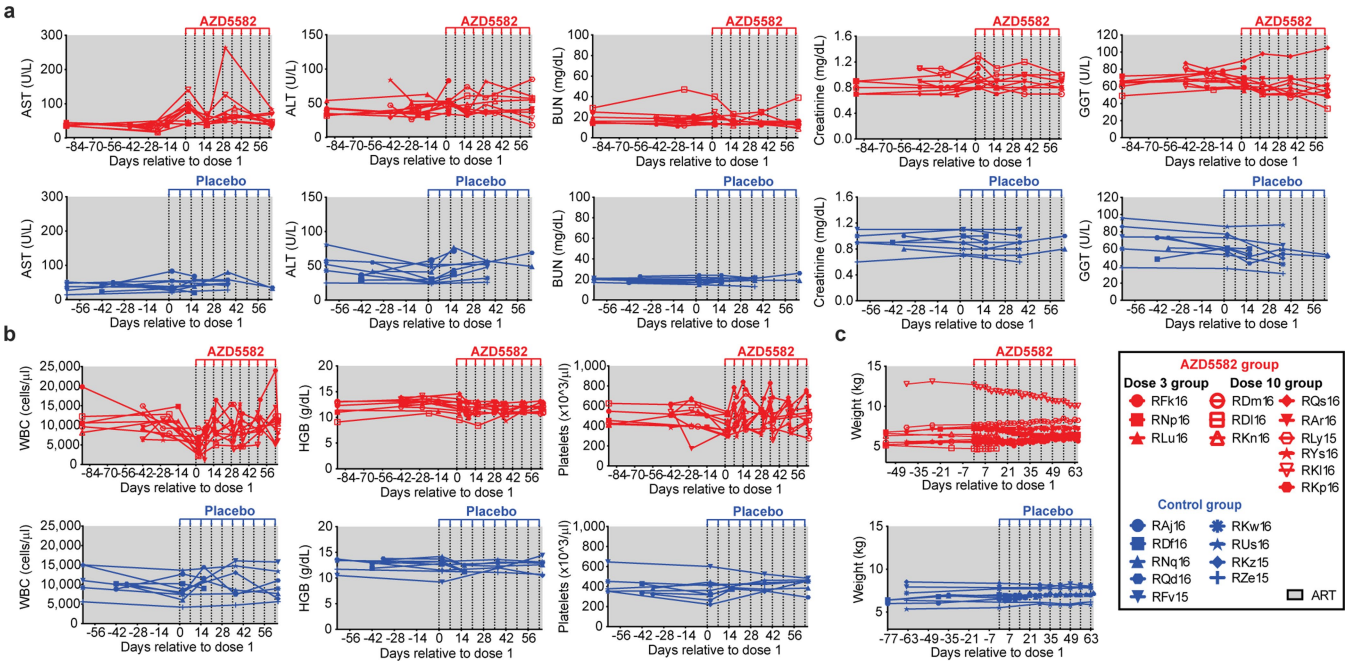

Extended Data Fig. 9 | AZD5582 can be safely administered in SIV-infected ART-suppressed rhesus macaques. a–**c**, Longitudinal assessment of serum chemistries (**a**), complete blood counts (**b**) and weight (**c**) of SIV-infected ART-treated rhesus macaques treated with AZD5582 (red, $n = 12$) compared with controls (blue, $n = 9$). Grey shading represents the period of ART administration. AST, aspartate aminotransferase; ALT, alanine aminotransferase; BUN, blood urea nitrogen; GGT, γ-glutamyltransferase; HGB, haemoglobin; WBC, white blood cell.

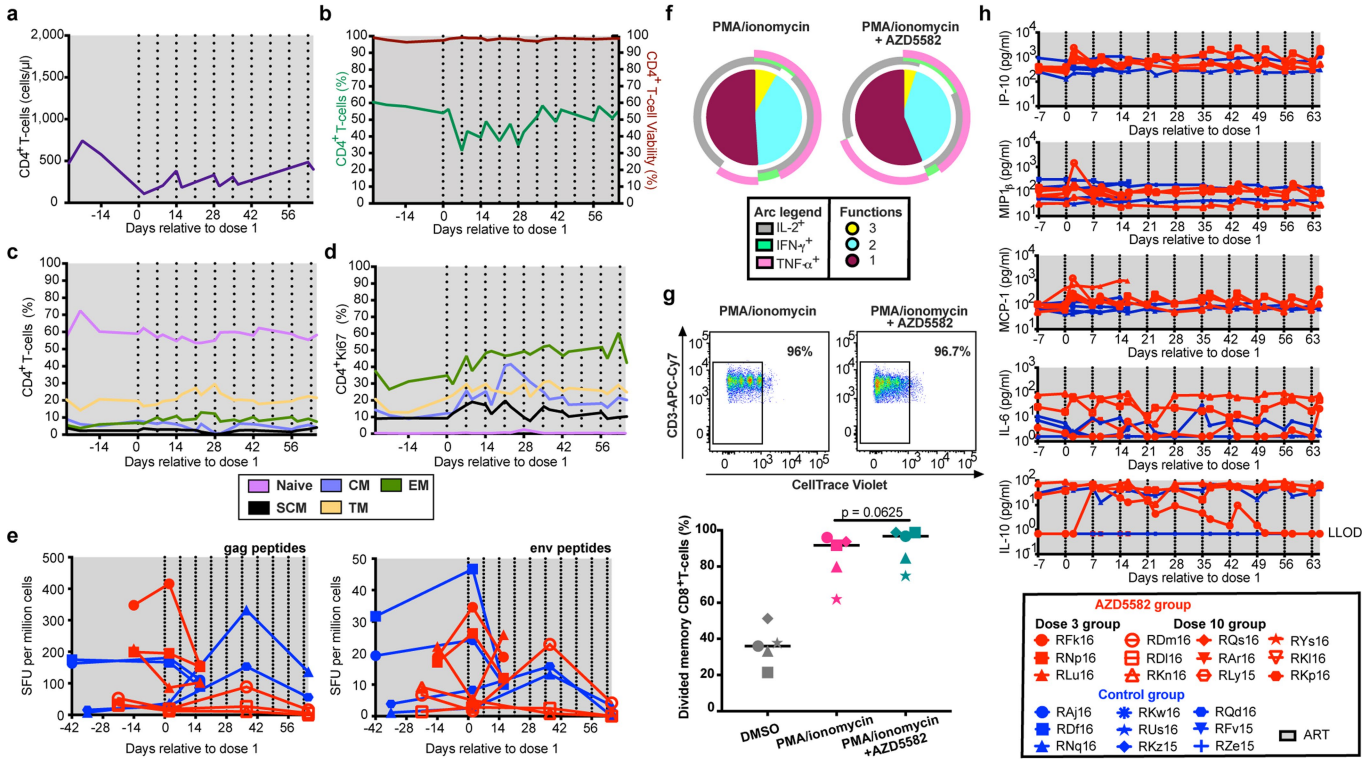

Extended Data Fig. 10 | Immunological effect of AZD5582 on SIV-infected ART-suppressed rhesus macaques. a, **b**, Longitudinal assessment of the count (**a**) and the frequency and viability (**b**) of CD4$^+$ T cells in SIV-infected ART-treated rhesus macaques during the period of AZD5582 treatment ($n = 12$). Lines represent median values. **c**, **d**, CD4$^+$ T cell naive and memory subset frequencies (**c**) and their expression of Ki-67 (**d**) in SIV-infected ART-treated rhesus macaques during the period of AZD5582 treatment ($n = 12$). Lines represent median values. **e**, SIV *gag*-specific (left) and SIV *env*-specific (right) CD8$^+$IFNγ$^+$ T cell responses in SIV-infected, ART-suppressed, AZD5582-treated (red, $n = 6$) and control (blue, $n = 4$) rhesus macaques. SFU, spot-forming units. **f**, Pie charts depicting the ability of memory CD8$^+$ T cells isolated from SIV-infected ART-suppressed control rhesus macaques ($n = 5$) to produce IFNγ, IL-2 and/or TNF in response to stimulation with PMA and ionomycin in the absence (left) or presence (right) of AZD5582 pre-treatment. **g**, Memory CD8$^+$ T cell proliferative response to stimulation with PMA and ionomycin with or without AZD5582 pre-treatment. Top, representative flow cytometry dot plots gated on memory CD8$^+$ T cells. Bottom, comparison between divided cells 5 days after stimulation in each group ($n = 5$ for each). Statistical significance was determined with a Wilcoxon matched-pairs signed-rank test. Horizontal lines represent the median. **h**, Longitudinal assessment of plasma levels of IP-10, MIP-1β, MCP-1, IL-6 and IL-10 by multiplex assay in SIV-infected ART-suppressed rhesus macaques treated with AZD5582 (red, $n = 6$) or control rhesus macaques (blue, $n = 4$). An additional four analytes (IFNγ, IL-8, IL-1β and IL-2) were undetectable in all macaques. **a**–**e**, **h**, Grey shading represents the period of ART administration. Dashed lines represent AZD5582 or placebo infusions. LLOD, lower limit of detection.